Article

Cell

CD10+GPR77+ Cancer-Associated Fibroblasts Promote Cancer Formation and Chemoresistance by Sustaining Cancer Stemness

Graphical Abstract

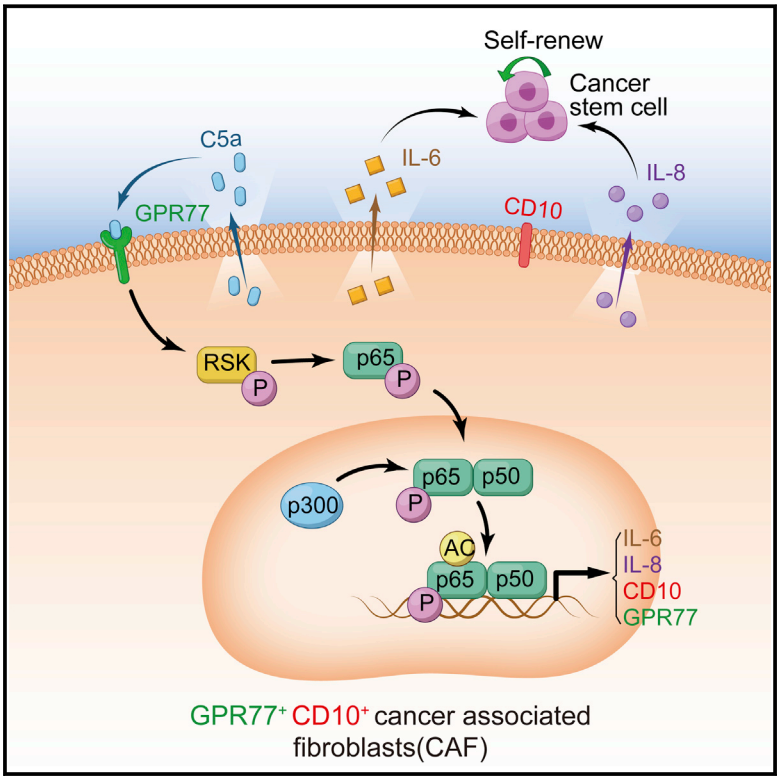

Highlights

- CD10 and GPR77 define a new CAF subset
- CD10+GPR77+ CAFs sustain cancer stemness and promote tumor chemoresistance
- Complement signaling maintains NF-κB activation
- Targeting CD10+GPR77+ CAFs restores chemosensitivity

Authors

Shicheng Su, Jianing Chen, Herui Yao, ..., Mengfeng Li, Qiang Liu, Erwei Song

Correspondence

songew@mail.sysu.edu.cn

In Brief

CD10 and GPR77 identify a cancer stemness-sustaining cancer-associated fibroblast subset.

Su et al., 2018, Cell *172*, 841–856
February 8, 2018
https://doi.org/10.1016/j.cell.2018.01.009

CellPress

Cell

CD10$^+$GPR77$^+$ Cancer-Associated Fibroblasts Promote Cancer Formation and Chemoresistance by Sustaining Cancer Stemness

Shicheng Su,[1,2,7] Jianing Chen,[1,2,7] Herui Yao,[3,7] Jiang Liu,[1,2] Shubin Yu,[1,2] Liyan Lao,[1,2] Minghui Wang,[4] Manli Luo,[1] Yue Xing,[1,2] Fei Chen,[1,2] Di Huang,[1,2] Jinghua Zhao,[1,2] Linbin Yang,[1,2] Dan Liao,[1,2] Fengxi Su,[1,2] Mengfeng Li,[5] Qiang Liu,[1,2] and Erwei Song[1,2,6,8,*]

[1]Guangdong Provincial Key Laboratory of Malignant Tumor Epigenetics and Gene Regulation, Medical Research Center, Sun Yat-Sen Memorial Hospital, Sun Yat-Sen University, Guangzhou 510120, China
[2]Breast Tumor Center
[3]Department of Oncology
[4]Department of Thoracic Surgery
Sun Yat-Sen Memorial Hospital, Sun Yat-Sen University, Guangzhou 510120, China
[5]Department of Microbiology and Key Laboratory of Tropical Disease Control
[6]Program of Molecular Medicine
Zhongshan School of Medicine, Sun Yat-Sen University, Guangzhou 510080, China
[7]These authors contributed equally
[8]Lead Contact
*Correspondence: songew@mail.sysu.edu.cn
https://doi.org/10.1016/j.cell.2018.01.009

SUMMARY

Carcinoma-associated fibroblasts (CAFs) are abundant and heterogeneous stromal cells in tumor microenvironment that are critically involved in cancer progression. Here, we demonstrate that two cell-surface molecules, CD10 and GPR77, specifically define a CAF subset correlated with chemoresistance and poor survival in multiple cohorts of breast and lung cancer patients. CD10$^+$GPR77$^+$ CAFs promote tumor formation and chemoresistance by providing a survival niche for cancer stem cells (CSCs). Mechanistically, CD10$^+$GPR77$^+$ CAFs are driven by persistent NF-κB activation via p65 phosphorylation and acetylation, which is maintained by complement signaling via GPR77, a C5a receptor. Furthermore, CD10$^+$GPR77$^+$ CAFs promote successful engraftment of patient-derived xenografts (PDXs), and targeting these CAFs with a neutralizing anti-GPR77 antibody abolishes tumor formation and restores tumor chemosensitivity. Our study reveals a functional CAF subset that can be defined and isolated by specific cell-surface markers and suggests that targeting the CD10$^+$GPR77$^+$ CAF subset could be an effective therapeutic strategy against CSC-driven solid tumors.

INTRODUCTION

Carcinoma-associated fibroblasts (CAFs) are activated fibroblasts (Orimo and Weinberg, 2006) constituting the major stromal components in many types of malignancies (Kalluri, 2016). Accumulating evidence suggests that CAFs play a crucial role in tumor development and are potential therapeutic targets for cancer. However, recent studies suggest that CAFs are heterogeneous and contain different subpopulations with distinct phenotypes and functions, which hinders their application in diagnosis and targeted therapy. Different CAF populations that secrete distinct profiles of cytokines have been identified in a variety of cancers (Öhlund et al., 2017; Sugimoto et al., 2006). Although significant prognostic impacts of CAFs have been studied in various tumors, including breast and lung cancers, whether CAFs are associated with good or poor prognosis is contradictory in different studies (Paulsson and Micke, 2014). More importantly, although it is generally thought that CAFs promote tumor progression, targeting CAFs leads to disease exacerbation in a cohort of pancreatic cancer patients (Amakye et al., 2013) and in a mouse model of pancreatic cancer (Özdemir et al., 2014; Rhim et al., 2014), suggesting that different fibroblast subsets may exert opposite functions in cancer progression. Therefore, to precisely target the cancer-promoting CAF subsets, it is necessary to identify specific markers to define these subpopulations and understand their functions and mechanisms. Although intracellular cytokine expression has been reported to characterize CAF subsets (Öhlund et al., 2017), the lack of specific cell-surface markers greatly impedes live-cell sorting for CAF subpopulations to investigate their functional heterogeneity and hampers the development of effective targeting therapy against cancer-promoting CAF subsets.

It has been shown that cancer stem cells (CSCs) are a key population of tumor cells that are highly tumorigenic and chemoresistant in many cancer types (Korkaya et al., 2012; Oskarsson et al., 2014; Yu et al., 2007). However, CSC markers are nonspecific or even unclear, which poses a great challenge to target

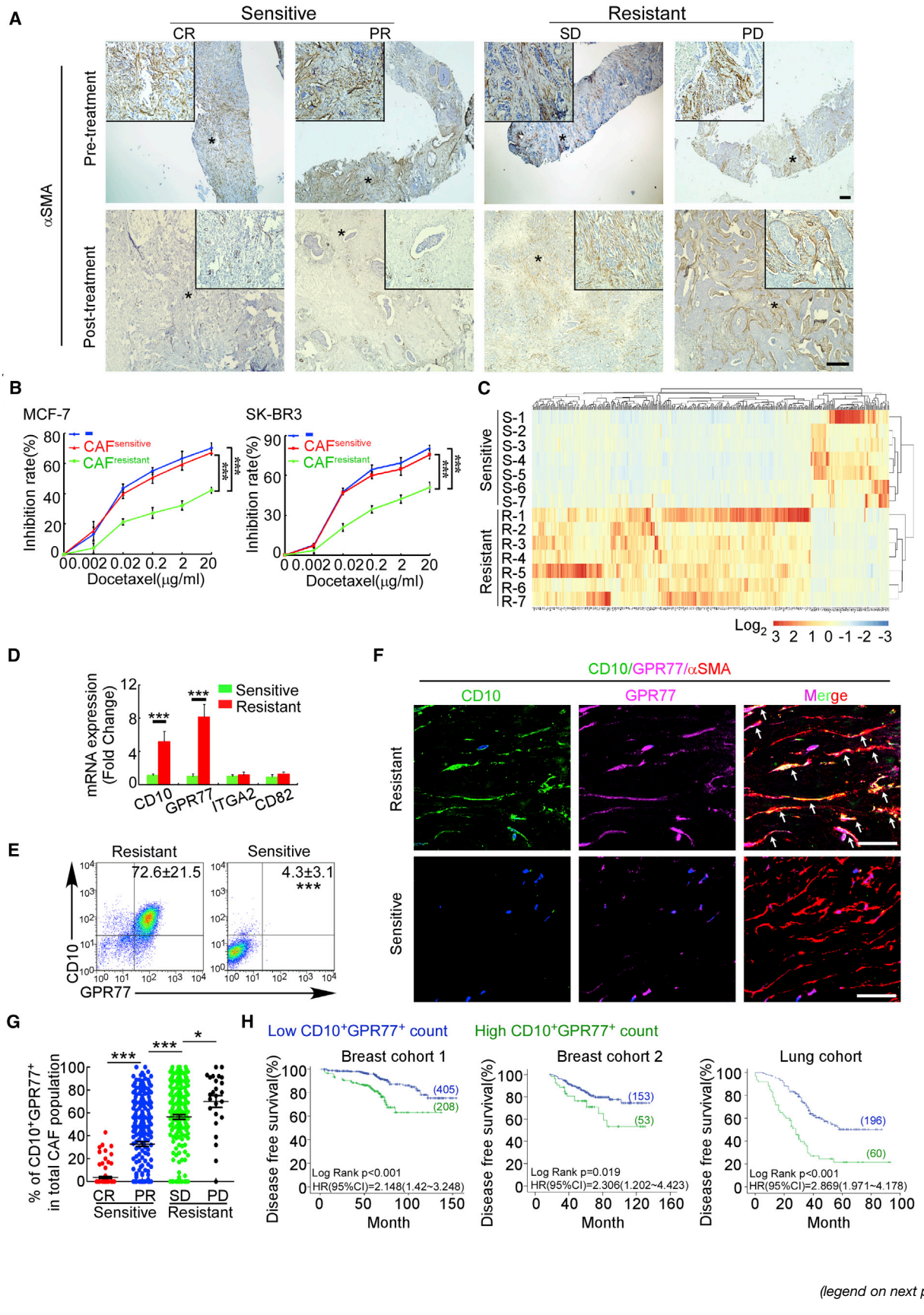

(legend on next page)

CSCs (Kreso and Dick, 2014). Like normal stem cells, the maintenance of CSC properties requires a supportive niche (Korkaya et al., 2011). Although fibroblasts are the central component of CSC niches (Vermeulen et al., 2010), only CAFs isolated from a fraction of breast cancer patients could enrich CSCs, suggesting the heterogeneous capacity of CAFs in supporting CSCs (Rudnick et al., 2011). Therefore, it is crucial to pinpoint the CAF subset that supports cancer stemness and to develop strategies to target these niche-forming fibroblasts for precision anti-CSC treatment. Here, we have shown that two cell-surface molecules can define a specific CAF subset that sustains cancer stemness and promotes tumor formation and chemoresistance. Targeting the CAF subset successfully abrogates tumor growth and reverses chemosensitivity.

RESULTS

A CAF Subset with High CD10 and GPR77 Expression Correlates with Chemoresistance and Poor Survival in Breast and Lung Cancer Patients

To study the contribution of CAFs to chemoresistance, we employed the clinical model of neo-adjuvant chemotherapy for breast cancer, wherein tumor shrinkage and tumor biology can be monitored during treatment (Prowell and Pazdur, 2012). We examined the number of activated fibroblasts, identified by immunohistochemistry for α-SMA and FAP, in paired primary tumor samples obtained from 578 breast cancer patients before and after neo-adjuvant chemotherapy. The number of CAFs in tumor samples obtained prior to chemotherapy by vacuum-assisted biopsies was not statistically different between patients who were sensitive and resistant, respectively, to chemotherapy (Figures 1A, S1A, and S1B). In contrast, following neo-adjuvant chemotherapy, CAFs were scarcely found in the residual tissues of the responsive patients with complete remission (n = 86). Additionally, CAF density in the residual tumors of the responsive patients with partial remission (n = 256) was markedly lower than that of the chemoresistant ones with disease progression and stable disease (n = 234) (Figures 1A, S1A, and S1C).

To investigate whether the heterogeneous CAFs contribute to chemoresistance, we isolated fibroblasts from seven chemoresistant breast cancer biopsies and seven chemosensitive ones obtained before neo-adjuvant chemotherapy (Figures S1D and S1E) (Orimo et al., 2005) and co-cultured them with breast cancer cell lines (MCF-7 and SK-BR3). When challenged with chemotherapeutic drugs, more tumor cells survived upon co-culturing with CAFs isolated from the chemoresistant samples, rather than CAFs from the chemosensitive ones, as compared with the tumor cells cultured alone (Figures 1B and S1F). These data suggested that chemoresistant and chemosensitive breast tumors contain functionally distinct CAF subtypes.

To further identify the molecular signatures for these functionally distinctive CAFs, we performed mRNA microarray analysis to compare the mRNA expression profiles of CAFs isolated from the primary tumor biopsies of seven sensitive patients and seven resistant ones before neo-adjuvant chemotherapy. Although CAFs from chemosensitive and resistant patients exhibited distinctive mRNA signatures (Figure 1C), conventional fibroblast markers, including α-SMA, PDGFRβ, FAP, FSP1, and collagen I, failed to distinguish them (Table S1). We then searched for cell-surface markers to identify these CAFs by evaluating differentially expressed mRNAs that encode membrane proteins and found four of them upregulated in the CAFs of the resistant tumors versus those derived from the sensitive ones. Among them, upregulation of CD10 and GPR77 in the CAFs from chemoresistant tumors was validated by qRT-PCR in another cohort of 24 patients (Figure 1D). Next, we confirmed that CD10 and GPR77 proteins were overexpressed in the CAFs of the chemoresistant tumors by flow cytometry (Figure 1E) and immunofluorescent staining (Figures 1F and 1G). Moreover, triple immunofluorescent staining of α-SMA, CD10, and GPR77

Figure 1. A CAF Subset with High CD10 and GPR77 Expression Correlates with Chemoresistance and Poor Survival in Breast and Lung Cancer Patients

(A) Representative images for immunohistochemical α-SMA staining in breast cancer biopsies before and resected samples after neo-adjuvant chemotherapy (n = 578). Asterisks indicate the area with higher magnification. The patients with complete remission (CR) or partial remission (PR) were classified as chemosensitive, while those with stable disease (SD) or progressive disease (PD) were chemoresistant. The positively stained blood vessels served as internal positive controls for α-SMA staining in the post-treatment complete remission sample.

(B) The growth inhibition of docetaxel on the MCF-7 and SK-BR3 cells cultured alone (–) or co-cultured with the CAFs isolated from chemoresistant and chemosensitive patients before neo-adjuvant chemotherapy. Three independent experiments were performed for the CAFs isolated from each of the seven chemoresistant and seven chemosensitive patients before neo-adjuvant chemotherapy.

(C) Heatmap representing differential expressed genes (fold change > 3) of the CAFs isolated from the biopsies of seven chemoresistant and seven chemosensitive patients before neo-adjuvant chemotherapy.

(D) The differential mRNA expression for cell-surface proteins was validated by qRT-PCR in CAFs isolated from pre-treatment breast cancer biopsies of chemosensitive (n = 13) and chemoresistant (n = 11) patients.

(E) Flow cytometric analysis of CD10 and GPR77 expression in the CAFs isolated from pre-treatment biopsies of chemosensitive (n = 11) and chemoresistant (n = 7) patients.

(F) Representative images of α-SMA, CD10, and GPR77 immunofluorescent staining in pre-treatment chemosensitive and chemoresistant breast cancer biopsies (n = 578).

(G) The percentage of $CD10^+GPR77^+$ CAFs in the total $\alpha\text{-SMA}^+$ CAFs in pre-treatment biopsies with different response to chemotherapy. CR, complete remission, n = 86; PR, partial remission, n = 258; SD, stable disease, n = 209; PD, progressive disease, n = 25.

(H) Kaplan-Meier survival curves of breast cancer and NSCLC patients with low and high infiltration numbers of $CD10^+GPR77^+$ CAFs in the discovery cohort (breast cohort 1, n = 613) and validation cohort (breast cohort 2, n = 206 and lung cohort, n = 256).

Mean ± SEM, $^{**}p < 0.01$; $^{***}p < 0.001$ by Student's t test. Scale bars, 50 μm.

See also Figure S1 and Table S1.

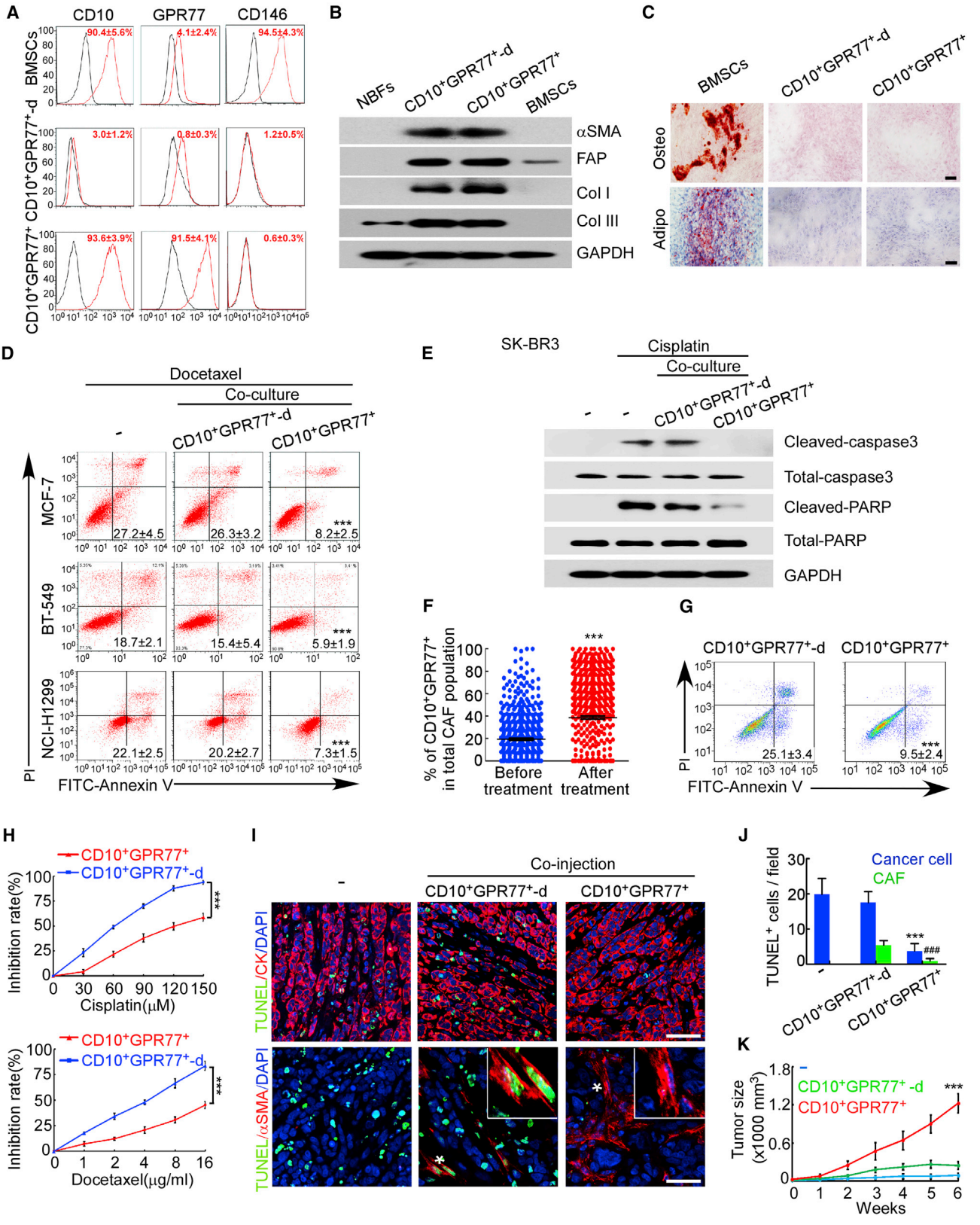

(legend on next page)

demonstrated that the percentage of $CD10^+GPR77^+$ CAFs ranged from 3% to 92% of the stromal fibroblasts in 613 cases of chemotherapy-naive surgical resected breast cancer samples (Figure S1G). More importantly, with an optimal cutoff point of 30% determined by X-tile statistical software, we found that the abundance of $CD10^+GPR77^+$ CAFs was associated with shorter patient survival, which was validated in an independent patient cohort (n = 206, Figure 1H). To further confirm this finding, we retrieved the mRNaseq data from the online breast cancer Hatzis dataset and divided the patients into two groups with or without both CD10 and GPR77 overexpression using X-tile. Consistent with the analysis using immunostaining, high expression of both genes was significantly associated with shorter metastasis-free survival in this independent dataset (Figure S1H).

To evaluate whether the clinical significance of $CD10^+GPR77^+$ CAF varies with the characteristics of breast cancer patients, we stratified the prognostic data by cancer subtyping, grading, and staging. In cohort 1, high $CD10^+GPR77^+$ CAF abundance was closely associated with shorter patient survival in the patients with ER^-HER2^-, ER^+HER2^-, and ER^+HER2^+ subtypes (Figure S1J). On the other hand, in the patients with ER^-HER2^+ breast cancer, a trend of shorter survival was also observed in those with high $CD10^+GPR77^+$ CAF infiltrating tumors, though the difference did not reach statistical significance (Figure S1J). Additionally, the disease-free survival of grade-3 breast cancer patients with high $CD10^+GPR77^+$ CAF infiltration was significantly shorter, while the one of grade-1/2 patients was independent of $CD10^+GPR77^+$ CAF infiltration. Furthermore, $CD10^+GPR77^+$ CAF abundance was associated with shorter patient survival in both stage I/II and III breast cancer (Figure S1J). Consistent with the immunostaining analysis, high expression of both CD10 and GPR77 gene was significantly associated with shorter metastasis-free survival in ER^-HER2^- (91.28% of which are triple-negative breast cancer) and grade-3 breast cancer patients in online Hatzis dataset (Figure S1K). Therefore, $CD10^+GPR77^+$ CAF infiltration in breast cancer is associated with shorter survival in multiple subtypes of the malignancy, particularly in the ER^-HER2^- and high-graded tumors.

In addition, we also evaluated $CD10^+GPR77^+$ CAF number in primary NSCLC samples from 256 patients. Our data showed that the NSCLC patients with higher numbers of $CD10^+GPR77^+$ CAFs in tumors exhibited shorter survival (Figure 1H). Furthermore, this finding was validated by three independent online datasets (Figure S1I). Together, our data showed that a specific human CAF subset associated with poor treatment outcome in breast and lung cancers can be marked by high expression of cell-surface CD10 and GPR77.

$CD10^+GPR77^+$ CAFs Induce Chemoresistance of Tumor Cells and Are Chemoresistant Themselves

Because CD10 is also expressed by bone-marrow derived mesenchymal stem cells (BMSCs) (Karnoub et al., 2007), which are potential CAF progenitors (Kalluri, 2016), we investigated whether these $CD10^+GPR77^+$ cells were BMSCs. We examined the expression of CD146, a marker for BMSCs but not expressed by fibroblasts (Covas et al., 2008). Flow cytometry showed that CD146 was absent in $CD10^+GPR77^+$ CAFs, while most BMSCs were CD146 positive (Figure 2A). In contrast, GPR77 and conventional myofibroblast markers were absent in BMSCs (Figure 2A and 2B). Functionally, unlike BMSCs, osteogenesis and adipogenesis were not observed in $CD10^+GPR77^+$ CAFs (Figure 2C). Collectively, the newly identified $CD10^+GPR77^+$ cells are an activated fibroblast subset, rather than BMSCs.

The distinct cell-surface markers of the $CD10^+GPR77^+$ CAFs allow us to purify the live fibroblast subset from clinical samples of breast and lung cancers by FACS and evaluate their chemoresistance-inducing function ex vivo. In agreement with the above data, the expression of conventional CAF markers,

Figure 2. $CD10^+GPR77^+$ CAFs Induce Chemoresistance of Tumor Cells and Are Chemoresistant Themselves

(A) Flow cytometric analysis for CD10, GPR77, and CD146 in $CD10^+GPR77^+$ CAFs and paired $CD10^+GPR77^+$-depleted ($CD10^+GPR77^+$-d) CAFs sorted from breast cancer samples (n = 5) and BMSCs from healthy donors (n = 5), mean ± SEM.

(B) Representative western blotting for α-SMA, FAP, collagen I, and collagen III in primary normal fibroblasts (NBFs), BMSCs, $CD10^+GPR77^+$ CAFs, and paired $CD10^+GPR77^+$-depleted CAFs (n = 3).

(C) Oil red O staining for adipogenic differentiation and Alizarin red S staining for osteogenic differentiation (n = 3). Scale bars, 50 μm.

(D) The proportion of apoptotic indicates cells treated with docetaxel, cultured alone (–), or co-cultured with indicated CAFs. The proportion of Annexin V^+/PI^- (early apoptosis) and Annexin V^+/PI^+ (late apoptosis) cells was shown.

Three independent experiments were performed for $CD10^+GPR77^+$ CAFs and paired $CD10^+GPR77^+$-depleted CAFs isolated from each of the eight breast (the top and middle row) and five NSCLC (the bottom row) patients. Mean ± SEM, ***$p < 0.001$ compared to tumor cells cultured alone ($^-$) by Student's t test.

(E) The expression of cleaved/total caspase-3 and PARP in cisplatin-treated SK-BR3 cells cultured alone or co-cultured with indicated CAFs (n = 3).

(F) The percentage of $CD10^+GPR77^+$ CAFs in breast cancer samples obtained before and after neo-adjuvant chemotherapy. n = 578; ***$p < 0.001$ by Student's t test.

(G) Apoptosis after cisplatin treatment in $CD10^+GPR77^+$ CAFs and paired $CD10^+GPR77^+$-depleted CAFs sorted from clinical breast cancer samples. The proportion of Annexin V^+ cells was shown.

(H) The growth inhibition rates of cisplatin and docetaxel on $CD10^+GPR77^+$ CAFs and paired $CD10^+GPR77^+$-depleted CAFs.

(G and H) Three independent experiments were performed for each of seven patients; mean ± SEM, ***$p < 0.001$ by Student's t test.

(I–K) MCF-7 cells with or without ($^-$) indicated CAFs were injected into mammary fat pads of NOD-SCID mice and treated with docetaxel (n = 8 per group).

(I) Representative immunofluorescent images for $TUNEL^+CK^+$ apoptotic tumor cells (top row) and $TUNEL^+$ α-SMA^+ apoptotic fibroblasts (bottom row) in xenografts. Scale bars, 50 μm.

(J) Quantitation of apoptotic tumor cells and fibroblasts in xenografts. ***$p < 0.001$ compared to tumor cells injected alone ($^-$); ###, $p < 0.001$ compared to tumor cells injected with $CD10^+GPR77^+$-depleted CAFs by Student's t test.

(K) Tumor growth curves. ***$p < 0.001$ compared to ($^-$) by Student's t test at week 6.

See also Figure S2.

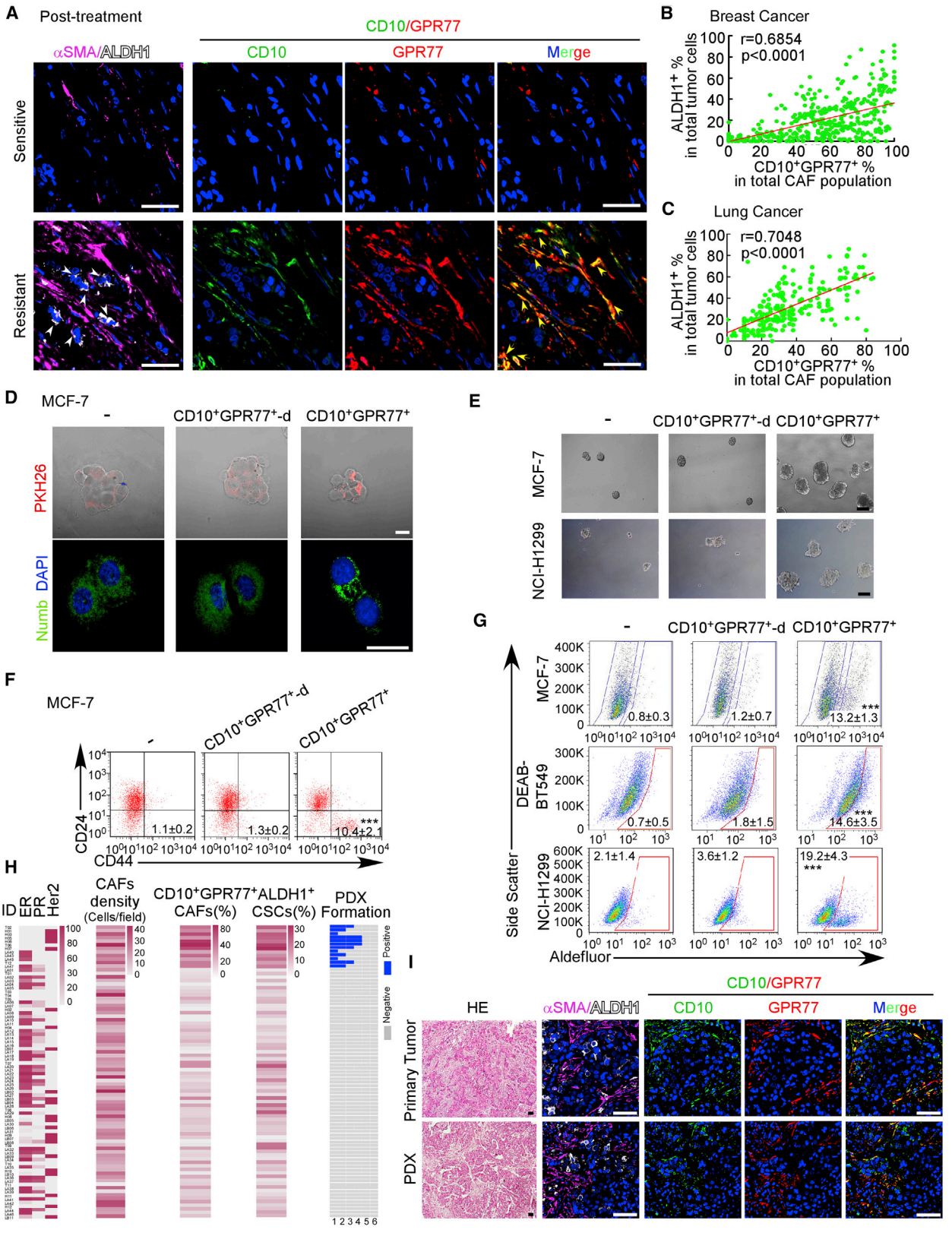

(legend on next page)

including α-SMA and FAP, is comparable between $CD10^+GPR77^+$ and $CD10^+GPR77^+$-depleted CAFs (Figures 2B and S2A), confirming that conventional CAF markers cannot distinguish these CAF subsets. We co-cultured breast and lung cancer cells with the primary $CD10^+GPR77^+$ CAFs isolated from breast and NSCLC patients, respectively, and challenged the tumor cells with docetaxel or cisplatin. Survival of the tumor cells under chemotherapy was dramatically enhanced upon co-culture with $CD10^+GPR77^+$ CAFs, rather than $CD10^+GPR77^+$-depleted CAFs (Figures S2B and S2C). Consistently, $CD10^+GPR77^+$ CAFs, rather than $CD10^+GPR77^+$-depleted CAFs, effectively protected both cancer cell lines and primary cancer cells from chemotherapy-induced apoptosis (Figures 2D and 2E and S2D–S2F). In agreement, following neoadjuvant chemotherapy, the percentage of $CD10^+GPR77^+$ CAFs was reversely associated with the percentage of apoptotic tumor cells, determined by TUNEL staining, in the samples of breast cancer patients (Figure S2G). On the other hand, we observed that neo-adjuvant chemotherapy enriched the proportion of $CD10^+GPR77^+$ CAFs in 578 cases of breast cancer patients (19.3% ± 0.9% before versus 38.7% ± 1.4% after chemotherapy, $p < 0.001$, Figure 2F), suggesting that these CAFs are insensitive to chemotherapy. Indeed, when the CAFs were challenged with docetaxel or cisplatin in vitro, the proportion of survived $CD10^+GPR77^+$ CAFs was much higher than that of the $CD10^+GPR77^+$-depleted CAFs (Figure 2G and 2H).

To verify the above findings in vivo, we employed a xenograft mouse model by co-injecting human CAFs and breast cancer cells into the mammary fat pads of immunocompromised mice (Figure S2H) as previously described (Orimo et al., 2005). Co-injection of MCF-7 cells with $CD10^+GPR77^+$ CAFs, but not $CD10^+GPR77^+$-depleted CAFs, dramatically reduced apoptosis of both cancer cells and fibroblasts (Figure 2I and 2J) and sustained tumor growth in mice under chemotherapy (Figure 2K). Similarly, co-injection of lung cancer A549 cells with $CD10^+GPR77^+$ CAFs isolated from lung cancer patients, but not $CD10^+GPR77^+$-depleted CAFs, substantially weakened the chemotherapeutic effects in vivo (Figure S2I). Collectively, these data suggested that $CD10^+GPR77^+$ CAFs are not only resistant to chemotherapy themselves, but also can induce chemoresistance of the tumor cells in their microenvironment.

$CD10^+GPR77^+$ CAFs Constitute a Supporting Niche for CSCs

Cancer stem cells (CSCs) are a key population of tumor cells that play a pivotal role in chemoresistance (Yu et al., 2007). In agreement, we found that the proportions of $ALDH1^+$ CSCs were higher in the chemoresistant samples versus the sensitive ones in the breast cancer biopsies obtained prior to neo-adjuvant chemotherapy (Figure S3A), which were further enriched following chemotherapy (Figure S3B). Here, we further investigated the correlation of $CD10^+GPR77^+$ CAFs and breast CSCs in the clinical samples. Interestingly, before and after neoadjuvant chemotherapy, the CSC proportions in the breast tumor samples were positively associated with the abundance of $CD10^+GPR77^+$ CAFs (Figures 3A, 3B, and S3C–S3F), and $CD10^+GPR77^+$ CAFs were found to surround the $ALDH1^+$ CSCs (Figures 3A and S3C), suggesting that this CAF subset may establish a supporting niche to sustain CSCs survival. Similarly, we also observed that $CD10^+GPR77^+$ CAFs surround the $ALDH1^+$ CSCs in the clinical samples of NSCLC (Figure S3G) and their numbers were positively associated (Figure 3C). Ex vivo assay showed that breast cancer cells co-cultured with $CD10^+GPR77^+$ CAFs, but not with $CD10^+GPR77^+$-depleted CAFs; demonstrated increased asymmetrical divisions (Figures 3D and S4A); and generated significantly more mammospheres than the untreated cells (Figures 3E and S4B). Additionally, the proportions of $ALDH1^+$ and $CD44^+CD24^-$ breast CSCs were markedly increased in both cancer cell lines and primary cancer cells upon co-culture with $CD10^+GPR77^+$ CAFs (Figures 3F, 3G, S4C, and S4D). Moreover, ABCG2 expression, an ABC family membrane (Takahashi et al., 2015), was increased in the tumor cells co-cultured with $CD10^+GPR77^+$ CAFs compared to those cultured alone or co-cultured with $CD10^+GPR77^+$-depleted CAFs (Figure S4E). Silencing ABCG2 by shRNAs significantly sensitized the tumor cells co-cultured with $CD10^+GPR77^+$ CAFs to chemotherapy (Figure S4F). Furthermore, co-culturing of the A549 and NCI-H1299 lung cancer cells with $CD10^+GPR77^+$ CAFs, rather than $CD10^+GPR77^+$-depleted CAFs, enhanced their sphere formation (Figures 3E and S4B) and increased $ALDH1^+$ proportions (Figures 3G and S4G).

In vivo, co-injection of $CD10^+GPR77^+$ CAFs isolated from breast cancer patients enhanced the tumorigenicity and the

Figure 3. $CD10^+GPR77^+$ CAFs Constitute a Supporting Niche for CSCs

(A) Representative images of α-SMA, ALDH1, CD10, and GPR77 immunofluorescent staining in serial sections of breast cancer samples after neo-adjuvant chemotherapy (n = 578). White arrows indicate $ALDH1^+$ cancer cells, and yellow arrows indicate $CD10^+$ $GPR77^+$ CAFs. Scale bars, 50 μm.

(B and C) The correlation between the percentage of $CD10^+GPR77^+$ CAFs and the percentage of $ALDH1^+$ tumor cells in breast cancer samples (n = 578) and lung cancer samples (n = 256).

(D–G) Tumor cells were cultured alone ($^-$) or co-cultured with indicated CAFs sorted from clinical samples of eight breast and five NSCLC patients, respectively. Three independent experiments were performed for each of the patients.

(D) Representative images of PKH26 and Numb immunofluorescent staining in MCF-7 cells. Scale bars, 50 μm.

(E) Representative images of sphere formation in MCF-7 and NCI-H1299 cells. Scale bars, 100 μm.

(F and G) The percentage of $CD44^+CD24^-$ (F) and $ALDH1^+$ (G) cells in the MCF-7, BT-549, and NCI-H1299 cells cultured alone ($^-$) or co-cultured with the indicated CAFs. Mean ± SEM, ***$p < 0.001$ compared to tumor cells cultured alone by Student's t test.

(H) The expression of ER/PR/Her2, the density of total CAFs, the percentage of $CD10^+GPR77^+$ CAFs and $ALDH1^+$ tumor cells in clinical samples from which PDXs were derived and the successful rates of PDX establishment in NOD/SCID mice (n = 82). Fresh tumor samples from each patient were implanted into six mice. Each blue box represents a successfully established PDX.

(I) Representative HE staining and immunostaining of human a-SMA, ALDH1, CD10, and GPR77 in serial sections of clinical samples (n = 82) and paired PDXs (n = 12) harvested from mice. Scale bars, 50 μm.

See also Figures S3 and S4.

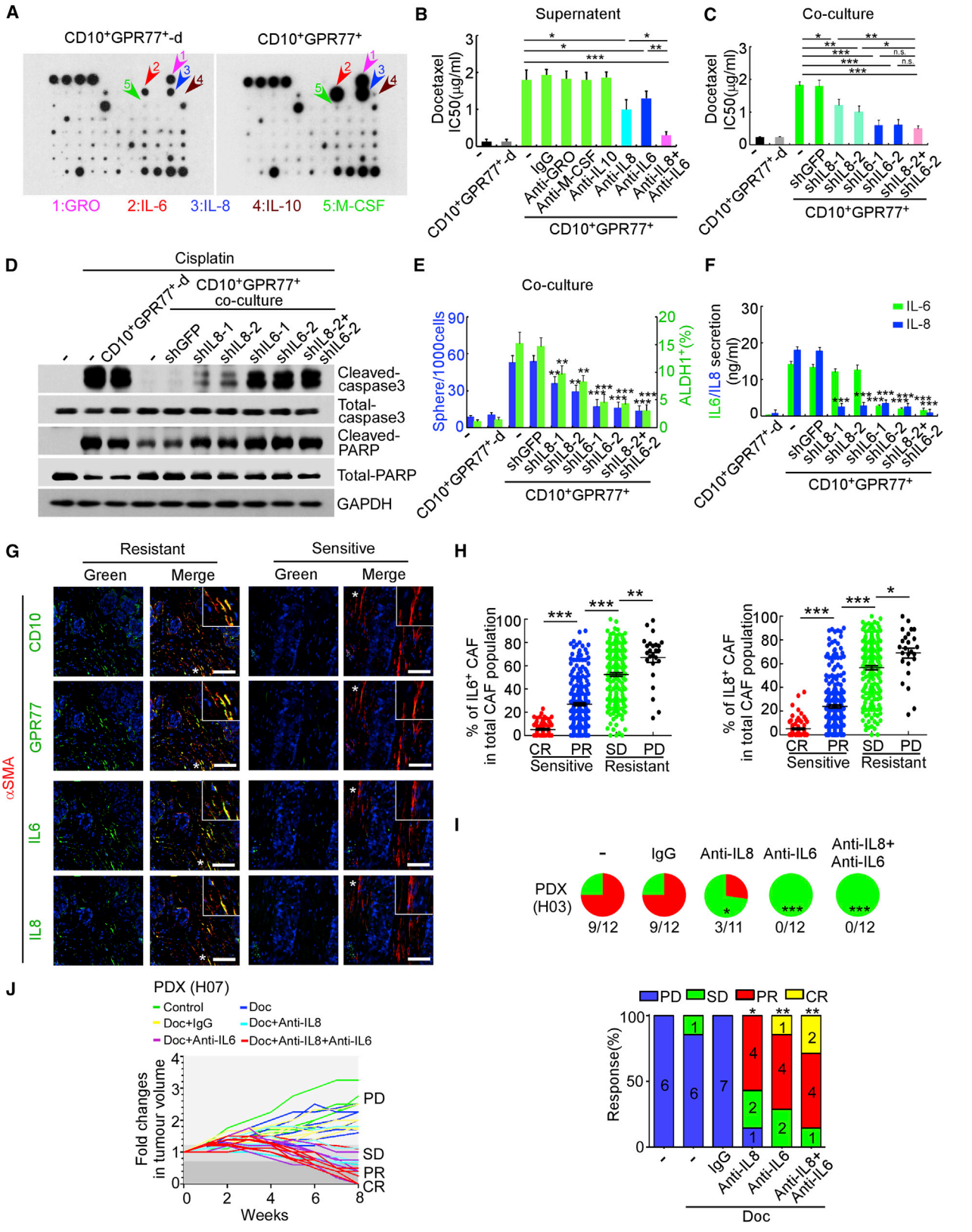

(legend on next page)

proportion of ALDH1$^+$ cancer cells upon serial transplantation of MCF-7 or primary breast cancer cells (Figures S4H–S4J). Similarly, tumor formation of the human lung cancer A549 cells in immunocompromised mice was also enhanced following co-inoculation with the CD10$^+$GPR77$^+$CAFs from human lung cancer samples (Figure S4K). To explore whether CD10$^+$GPR77$^+$ CAFs contribute to the capacity of tumor formation in a more patient-relevant in vivo model of patient-derived xenografts (PDX) (Byrne et al., 2017), we implanted fresh primary tumor samples resected from 82 breast cancer patients orthotopically into the cleared mammary fat pads of the immunocompromised NOD.SCID mice and correlated the proportions of CD10$^+$ GPR77$^+$ CAFs with the successful rate of PDX establishment. The clinical samples covered a board range of patient clinicopathological features and molecular subtypes (Figure 3H). 12 out of 82 (~14.6%) cases successfully established PDX in the mice (Figure 3H), and the pathological features of the PDX were analogous to the primary tumors (Figure 3I). More importantly, the number of human CD10$^+$GPR77$^+$ CAFs in both the clinical samples resected from breast cancer patients and the paired PDXs harvested from the mice was positively associated with the CSC proportions (Figures 3I, S4L, and S4M), and primary tumor tissues containing a higher percentage of CD10$^+$GPR77$^+$ CAFs, rather than total CAFs, had higher successful PDX engraftment rates (Figures 3H and S4N). Therefore, the abundance of CD10$^+$GPR77$^+$ CAFs in breast cancer stroma contributes to successful PDX establishment and the capacity of tumor formation by enriching CSCs.

CD10$^+$GPR77$^+$ CAFs Induce CSCs Enrichment and Chemoresistance by Secreting IL-6 and IL-8

To understand how CD10$^+$GPR77$^+$ CAFs exert their functions, we compared the cytokine profiles secreted by CD10$^+$GPR77$^+$ CAFs and CD10$^+$GPR77$^+$-depleted CAFs using antibody microarrays and identified a panel of cytokines abundantly produced by the CD10$^+$GPR77$^+$ CAFs (Figure 4A). Among them, IL-6 and IL-8 have been reported to mediate CSCs enrichment and chemoresistance (Meads et al., 2009). Indeed, treating the co-cultures of CD10$^+$GPR77$^+$ CAFs and breast cancer cells with neutralizing antibodies against IL-6 or/and IL-8, but not with antibodies against IL-10, GRO, or MCSF, potently abrogated the effects of the CAFs in CSCs enrichment and chemoresistance induction (Figures 4B and S5A–S5C). Interestingly, while silencing IL-8 in CD10$^+$GPR77$^+$ CAFs only partially reduced their effects to enrich CSCs and to induce chemoresistance in the co-cultured tumor cells, IL-6 knockdown almost completely abrogated these effects, which was nearly equivalent to the effect of silencing both cytokines (Figures 4C–4E and S5D–S5F). Consistently, silencing IL-8 in CD10$^+$GPR77$^+$ CAFs did not influence IL-6 production, but silencing IL-6 almost completely abrogated IL-8 secretion (Figure 4F), suggesting that IL-8 production by CD10$^+$GPR77$^+$ CAFs is dependent on IL-6. In vivo, IL-8 knockdown in CD10$^+$GPR77$^+$ CAFs significantly repressed tumorigenesis and CSCs enrichment of the co-injected cancer cells, while silencing IL-6 or both cytokines almost completely abolished these effects (Figures S5G and S5H).

In agreement, we observed that both IL-6 and IL-8 were abundantly expressed in CD10$^+$GPR77$^+$ CAFs of the clinical samples from breast cancer patients who were refractory to neo-adjuvant chemotherapy, determined by immunofluorescent staining in the serial sections (Figures 4G and 4H). To further investigate whether the abundant IL-6/IL-8 production in CD10$^+$GPR77$^+$ CAFs was responsible for successful PDX establishment, we implanted primary breast tumor samples containing high proportions of CD10$^+$GPR77$^+$ CAFs (>30%) into the immunocompromised mice and administrated IL-6

Figure 4. CD10$^+$GPR77$^+$ CAFs Induce CSCs Enrichment and Chemoresistance by Secreting IL-6 and IL-8

(A) Representative cytokine arrays for CD10$^+$GPR77$^+$ CAFs and paired CD10$^+$GPR77$^+$-depleted CAFs; arrows indicate the cytokines with significant changes (n = 5).

(B) IC_{50} of docetaxel in MCF-7 cells that were pre-incubated with the supernatants of CD10$^+$GPR77$^+$ CAFs without ($^-$) or with indicated neutralizing antibody and then treated with docetaxel. Mean ± SEM, *p < 0.05, **p < 0.01 and ***p < 0.001 by Student's t test.

(C–F) MCF-7 cells were cultured alone ($^-$) or co-cultured with indicated CAFs.

(C) IC_{50} of docetaxel in the MCF-7 cells cultured alone ($^-$) or co-cultured with the indicated CAFs. Mean ± SEM, *p < 0.05, **p < 0.01 and ***p < 0.001 by Student's t test.

(D) The apoptosis of cisplatin-treated SK-BR3 cells was determined by western blotting for cleaved caspase-3 and PARP.

(E) The proportions of mammosphere formation and ALDH1 positive cells in MCF-7 cells without or with indicated coculture. Mean ± SEM, **p < 0.01, and ***p < 0.001 compared with MCF-7 cells co-cultured with untreated CD10$^+$GPR77$^+$ CAFs by Student's t test.

(F) ELISA for IL-6 and IL-8 levels in the supernatants of indicated CAFs. Mean ± SEM, ***p < 0.001 compared with untreated CD10$^+$GPR77$^+$ CAFs by Student's t test.

(G) Representative images of α-SMA, CD10, GPR77, IL6, and IL8 immunostaining in serial sections of resistant or sensitive breast cancer samples before neoadjuvant chemotherapy (n = 578). Scale bars, 50 μm.

(H) Quantification of IL6 and IL8 immunostaining on CAFs in breast cancer biopsies section before neo-adjuvant chemotherapy. Mean ± SEM, *p < 0.05, **p < 0.01, ***p < 0.001 by Student's t test.

(I) Clinical breast cancer samples with high proportions of CD10$^+$GPR77$^+$ CAFs (H03, 47%) were implanted into NOD.SCID mice receiving control IgG or IL-6 or/and IL-8 neutralizing antibodies. n = 12 per group except for anti-IL-8 group (n = 11). *p < 0.05, ***p < 0.001 compared with the untreated groups ($^-$) by Fisher's exact test.

(J) The fold changes in tumor size and response rates in PDX (H07) that received treatments of docetaxel and IL-6 or/and IL-8 neutralizing antibodies. n = 7 per group except for control group (n = 6). The therapeutic responses were evaluated using the RECIST standard. *p < 0.05, **p < 0.01 compared with the docetaxel treated group ($^-$) by Fisher's exact test.

(B), (C), (E), and (F) Three independent experiments were performed for each of the five patients. (D) Representative images from two replicates for each of the three patients.

See also Figure S5.

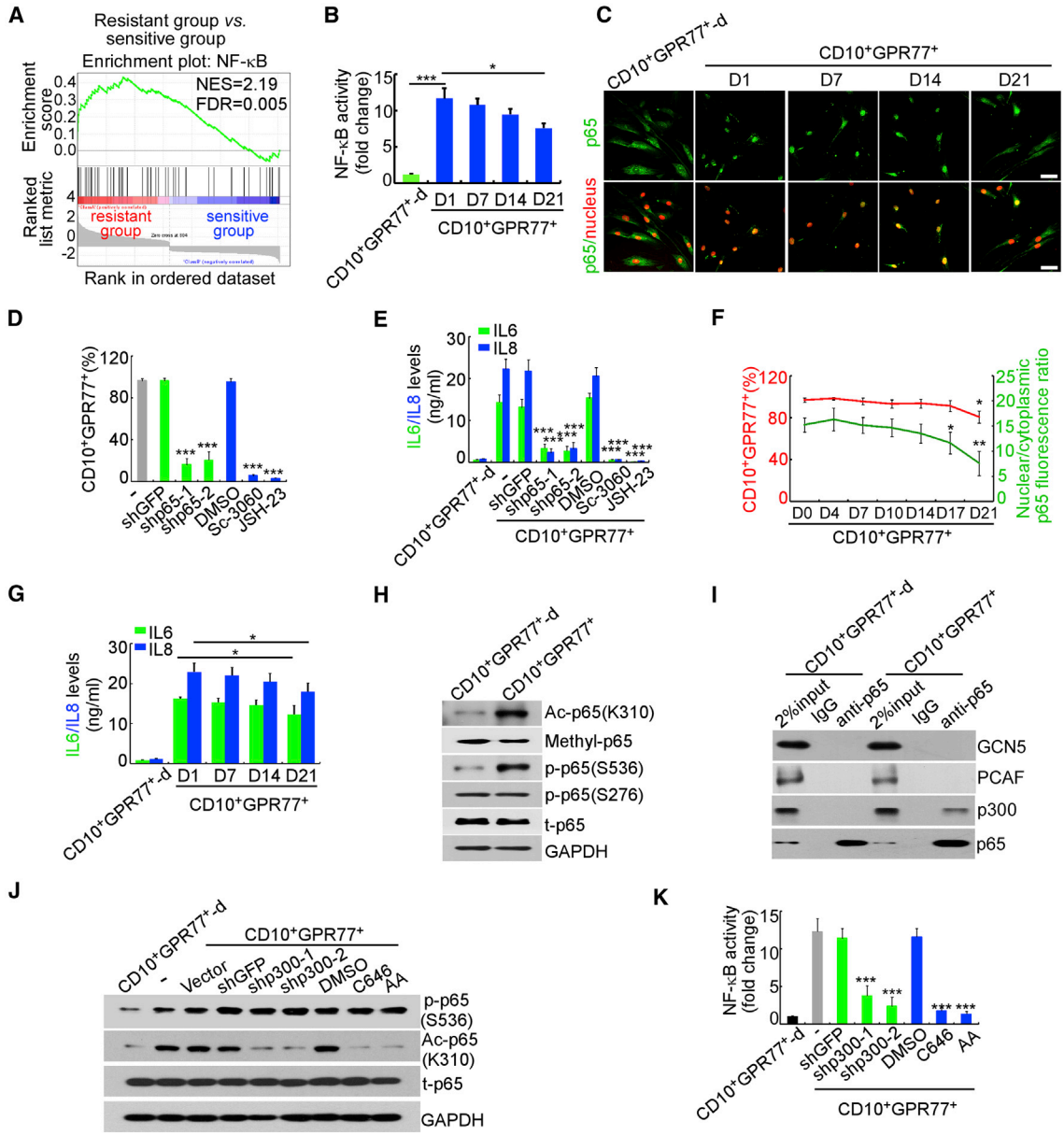

Figure 5. Prolonged NF-κB Activation via P300-Mediated P65 Acetylation Maintains the Phenotypes and Functions of CD10$^+$GPR77$^+$ CAFs

(A) GSEA analysis revealed an enrichment of NF-κB target genes in the CAFs from chemoresistant breast cancer samples. The heatmap of differential expression profiles was illustrated in Figure 1C.

(B, C, and G) CD10$^+$GPR77$^+$ CAFs were cultured for indicated days. Paired CD10$^+$GPR77$^+$-depleted CAFs at day 1 were used as controls. Luciferase reporter assays showed the NF-κB activity (B), immunofluorescent p65 staining showing its nuclear translocation (C), and their IL-6 and IL-8 levels (G).

(D and E) CD10$^+$GPR77$^+$ CAFs were transduced without ($^-$) or with GFP-shRNA or p65 shRNA or pretreated with inhibitors of NF-κB nuclear translocation. Quantitation of the percentage of CD10$^+$GPR77$^+$ CAFs (D) and the IL-6 and IL-8 levels (E) were shown.

(F) CD10$^+$GPR77$^+$ CAFs were cultured for indicated days. Flow cytometry showed the percentage of CD10$^+$GPR77$^+$ CAFs, and the ImageJ software analysis showed the nuclear/cytoplasmic ratio of p65 immunofluorescence intensity. *$p < 0.05$, **$p < 0.01$ compared with day 0 (D0) CD10$^+$GPR77$^+$ CAFs by Student's t test.

(H) The expression of total, Lys310 acetylation (ac), methylation (methyl), Ser536 and Ser276 phosphorylation of p65 in indicated CAFs was determined by western blot.

(I) Interactions of p65 with HAT molecules (GCN5, PCAF and p300) in indicated CAFs were determined by immunoprecipitation.

(J and K) CD10$^+$GPR77$^+$ CAFs were transduced without ($^-$) or with p300 shRNA or were pretreated with p300 inhibitors (C646 or anacardic acid [AA], DMSO served as a negative control).

(J) The modifications of Ser536 phosphorylation and Lys310 acetylation of p65 were determined by western blot.

(legend continued on next page)

or/and IL-8 neutralizing antibodies. Strikingly, PDX establishment was significantly retarded by IL-8 neutralization, and no PDX growth was observed in the mice treated with anti-IL-6 antibody or both anti-IL-6 and anti-IL-8 antibodies (Figure 4I). Furthermore, combined treatment of the mice with anti-IL-8 neutralizing antibody and docetaxel improved the chemotherapeutic response, while combination of anti-IL-6 neutralizing antibody or both antibodies with chemotherapy almost completely eradiated the PDXs in the mice (Figure 4J). Collectively, these data suggest that $CD10^+GPR77^+$ CAFs enrich CSCs, enhance tumor formation of PDXs, and induce cancer chemoresistance by secreting IL-6 and IL-8, while the effect of IL-8 depends on autocrine IL-6.

Prolonged NF-κB Activation via P300-Mediated P65 Acetylation Maintains the Phenotypes and Functions of $CD10^+GPR77^+$ CAFs

To unravel the signaling pathways activated in $CD10^+GPR77^+$ CAFs that sustained the production of IL-6 and IL-8, we performed gene set enrichment analysis (GSEA) for the microarray data of the CAFs isolated from chemosensitive and resistant tumor biopsies. We found that a panel of NF-κB target genes were upregulated in the CAFs isolated from chemoresistant samples, including IL-6 and IL-8 (Figure 5A), which was further verified by qRT-PCR (Figure S6A). Additionally, NF-κB binding sites upstream of the CD10- and the GPR77-expressing cassettes were confirmed, respectively, by chromatin immunoprecipitation (ChIP) analysis with anti-p65 antibody (Figures S6B and S6C), suggesting that CD10 and GPR77 that mark the fibroblast subset are also NF-κB target genes. In agreement, enhanced NF-κB transcription activities and increased p65 nuclear translocation were observed in $CD10^+GPR77^+$ CAFs (Figures 5B and 5C), but phosphorylation of IKK and IκB was not increased as compared with the $CD10^+GPR77^+$-depleted CAFs (Figure S6D). Furthermore, either inhibitors for NF-κB nuclear translocation (Sc-3060 and JSH-23) or p65 shRNA, but not the IKK inhibitors (BAY 11-7082 and BMS-345541), efficiently abrogated CD10 and GPR77 overexpression (Figure 5D, S6E, and S6F), as well as IL-6 and IL-8 production (Figures 5E and S6G), suggesting that NF-κB signaling is responsible for the phenotype and function of $CD10^+GPR77^+$ CAFs.

We next evaluated whether the phenotype mediated by NF-κB activation in $CD10^+GPR77^+$ CAFs was sustainable. Upon culturing $CD10^+GPR77^+$ CAFs ex vivo, nuclear translocation of p65 (Figure 5C and 5F), transcription activity of NF-κB (Figure 5B), overexpression of CD10 and GPR77 (Figure 5F), and IL-6 and IL-8 production (Figure 5G) were maintained for at least 14 days, while phosphorylation of IKK and IκBα remained at low levels (Figure S6D), suggesting that p65 nuclear retention was independent of upstream IKK or IκB activities. To further understand the mechanisms responsible for maintaining high NF-κB activities in these cells, we examined the modification of p65 protein, as methylation and acetylation of p65 were previously shown to maintain p65 nuclear retention (Chen et al., 2001). Western blotting demonstrated that p65 acetylation at K310, but not methylation, was markedly enhanced in $CD10^+GPR77^+$ CAFs (Figure 5H). Since p65 acetylation requires its phosphorylation (Chen and Greene, 2004), we examined p65 phosphorylation using western blot. Although IKK or IκB phosphorylation remains at low levels, p65 phosphorylated at S536, but not S276, was markedly increased in this CAF subset (Figure 5H), suggesting that the sustained NF-κB activation with p65 phosphorylation and acetylation in the CAFs was maintained via other signaling molecules but IKK activation.

Furthermore, to identify the histone acetyltransferase (HAT) responsible for p65 acetylation, we performed immunoprecipitation using p65 antibody. Among all the HAT molecules, immunoprecipitation revealed that p65 interacted with p300 in the $CD10^+GPR77^+$ CAFs, but not in the $CD10^+GPR77^+$-depleted CAFs (Figure 5I). More importantly, shRNA-mediated silencing or pharmaceutical suppression of p300 significantly reduced p65 acetylation (Figure 5J) but did not influence p65 phosphorylation (Figure 5J). Additionally, suppression of p300 reduced p65 nuclear accumulation (Figure S6H), NF-κB activation (Figure 5K), CD10 and GPR77 overexpression (Figure S6I), and IL-6 as well as IL-8 production (Figure S6J). Thus, the interaction of p65 with p300 leads to its acetylation at K310 but does not influence its phosphorylation in the CAF subset.

GPR77-Induced P65 Phosphorylation Is Prerequisite for Its Acetylation and Sustains NF-κB Activation in $CD10^+GPR77^+$ CAFs

Next, we further evaluated whether CD10 or GPR77 that marks the CAF subset may play a role in maintaining the functions and signaling pathways of $CD10^+GPR77^+$ CAFs. Surprisingly, knocking down GPR77, but not CD10, substantially reduced secretion of IL-6 and IL-8 (Figure 6A), inhibited NF-κB activity (Figure 6B), and reduced nuclear retention of p65 (Figure 6C), which was accompanied by decreased S536 phosphorylation and K310 acetylation, but not S276 phosphorylation, of p65 protein (Figure 6D). Since K310 acetylation in p65 requires its phosphorylation at S536, which can be induced by IKK or RSK1 phosphorylation (Chen and Greene, 2004), we further investigated whether IKK or RSK1 was associated with the GPR77-induced p65 phosphorylation. We found that RSK1 phosphorylation was markedly elevated in $CD10^+GPR77^+$ CAFs compared to $CD10^+GPR77^+$-depleted CAFs and could be completely inhibited by silencing GPR77 (Figure 6D). In contrast, knocking down GPR77 did not result in appreciable change in IKK phosphorylation, which remained at low level in $CD10^+GPR77^+$ CAFs (Figure 6D). More importantly, shRNA-mediated silencing of GPR77 in $CD10^+GPR77^+$ CAFs dramatically abrogated their ability to enrich CSCs and induce

(K) Luciferase reporter assays for NF-κB activity.

(B–G) and (K) Three independent experiments were performed for each of the four patients. (H–J) Representative images from two replicates from each of the three patients. Mean ± SEM, $p < 0.05$, $^{**}p < 0.01$, $^{***}p < 0.001$ compared with untreated $CD10^+GPR77^+$ CAFs by Student's t test unless stated otherwise. See also Figure S6.

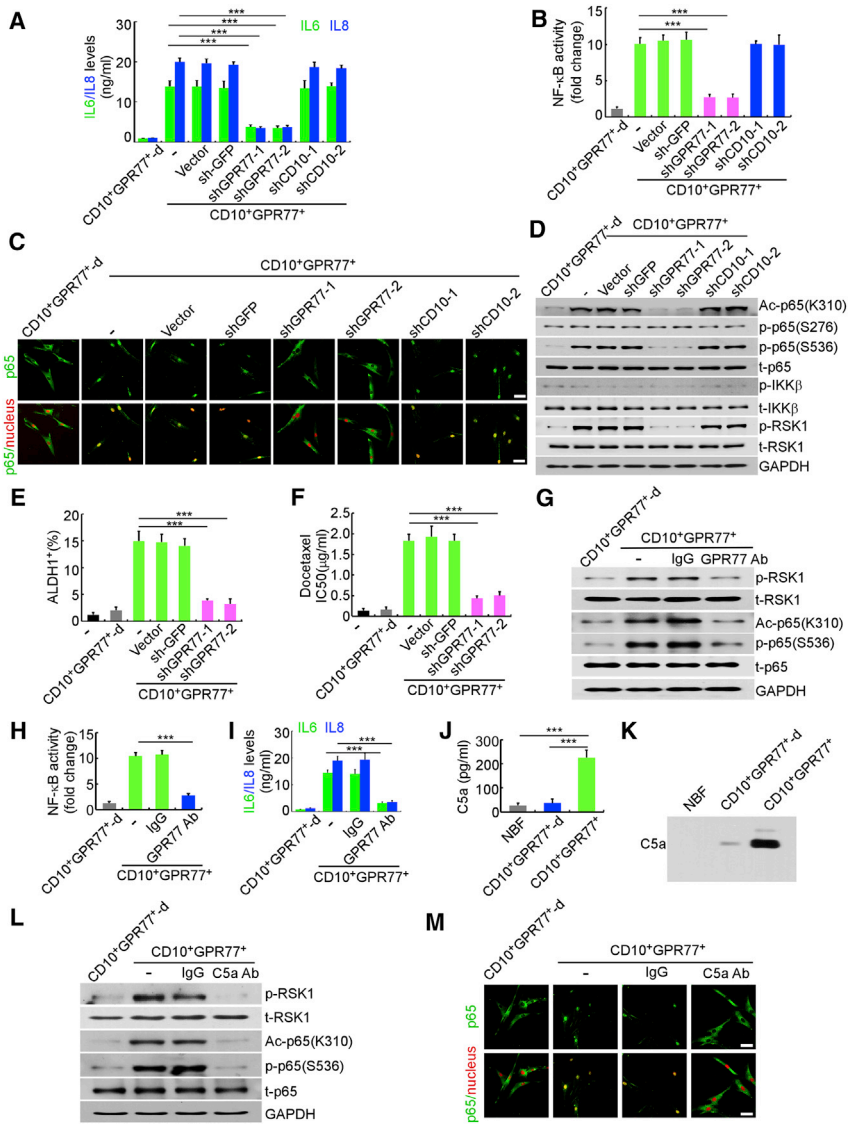

Figure 6. GPR77-Induced P65 Phosphorylation Is Prerequisite for Its Acetylation and Sustains NF-κB Activation in CD10$^+$GPR77$^+$ CAFs

(A–D) CD10$^+$GPR77$^+$ CAFs were transduced without ($^-$) or with shRNA for GPR77 or CD10.

(A) The IL-6 and IL-8 levels detected by ELISA.

(B) NF-κB activity detected by luciferase reporter assays.

(C) Representative immunofluorescent images of p65 nuclear translocation. Scale bars, 50 μm.

(D) Western blotting for indicated proteins.

(E and F) MCF-7 cells were co-cultured with CD10$^+$GPR77$^+$ CAFs transduced without ($^-$) or with shRNA for GPR77. The percentage of ALDH1$^+$ cancer cells (E) and IC_{50} of docetaxel in MCF-7 cells were shown (F).

(G–I) RSK1 phosphorylation as well as Lys310 acetylation and S536 phosphorylation of p65 (G), NF-κB activity (H), and IL-6/IL-8 production (I) of CD10$^+$GPR77$^+$ CAFs pretreated with control IgG or anti-GPR77 neutralizing antibody.

(J and K) The production of C5a in the supernatants of CD10$^+$GPR77$^+$-depleted CAFs and CD10$^+$GPR77$^+$ CAFs was detected by ELISA (J) and western blot (K).

(L and M) CD10$^+$GPR77$^+$ CAFs were treated with control IgG or anti-C5a neutralizing antibody. Indicated proteins were determined by western blot (L), and p65 nuclear translocation was determined by immunofluorescent staining (M). Scale bars, 50 μm.

(A–C), (E and F), (H–J), and (M) Three independent experiments were performed for CAFs isolated from each of the four patients. (D), (G), (K), and (L) Two replicates for each of the three patients. Mean ± SEM, ***$p < 0.001$ by Student's t test.

See also Figure S7.

chemoresistance in the co-cultured MCF-7 breast cancer cells (Figure 6E and 6F).

In agreement, blocking GPR77 with a neutralizing antibody effectively abrogated RSK1 phosphorylation, which was accompanied by inhibition of p65 phosphorylation, acetylation (Figure 6G), and nuclear accumulation (Figure S7A). Additionally, anti-GPR77 neutralizing antibody dramatically suppressed the activity of NF-κB (Figure 6H), IL-6, and IL-8 secretion (Figure 6I); chemoresistance induction (Figure S7B); and CSC enrichment (Figure S7C) in CD10$^+$GPR77$^+$ CAFs to the levels of the CD10$^+$GPR77$^+$-depleted CAFs.

Since GPR77 is a receptor for complement C5a (Rittirsch et al., 2008), we further evaluated whether CAFs produce the complement for self-sustaining GPR77 signaling. We observed that CD10$^+$GPR77$^+$ CAFs produced a considerably higher amount of C5a compared to CD10$^+$GPR77$^+$-depleted CAFs (Figures 6J and 6K). Moreover, neutralization C5a inhibited RSK1 phosphorylation, p65 phosphorylation, and acetylation (Figure 6L); p65 nuclear accumulation (Figure 6M); NF-κB activation (Figure S7D); and IL-6 and IL-8 production (Figure S7E) in CD10$^+$GPR77$^+$ CAFs. In addition, C5a secretion was markedly reduced by NF-κB inhibition (Figure S7F), suggesting that NF-κB also controls C5a production in CD10$^+$GPR77$^+$ CAFs.

Treatment of Breast Cancer PDXs with Anti-GPR77 Inhibits Tumorigenesis and Enhances Chemotherapeutic Effects

We further investigated the therapeutic potential of anti-GPR77 neutralizing antibody to breast cancer in the PDXs implanted into immunocompromised mice. Notably, treatment with anti-GPR77 antibody, but not the isotype IgG, nearly abolished PDX establishment in the immunocompromised mice (Figure 7A).

To evaluate whether blocking GPR77 may reverse chemoresistance in breast cancers with high infiltration of CD10$^+$GPR77$^+$ CAFs, we combined chemotherapy with anti-GPR77 neutralizing antibody after the PDXs were established. Combined treatment of docetaxel with anti-GPR77 antibody significantly reduced the

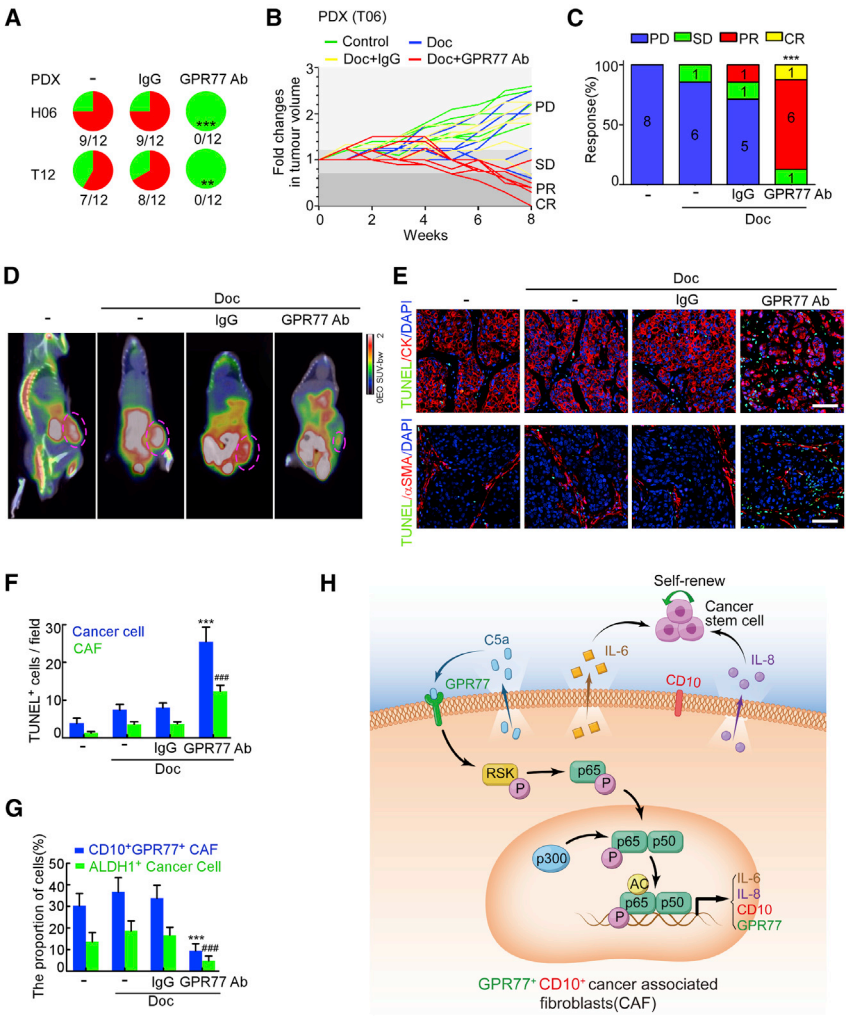

Figure 7. Treatment of Breast PDXs with Anti-GPR77 Abolishes Tumorigenesis and Enhances Chemotherapeutic Effects

(A) Clinical breast cancer samples (H06, T12) were implanted into NOD.SCID mice, and GPR77 neutralizing antibody was administrated concomitantly and repeated every 3 days. PDX formation rates after 12 weeks were shown. n = 12 per group, $^{*}p < 0.05$, $^{**}p < 0.01$, $^{***}p < 0.001$ compared with untreated groups by Fisher's exact test.

(B–G) Clinical breast cancer samples (T06) were implanted in NOD/SCID. Combined treatment of docetaxel and GPR77 neutralizing antibody was administrated. n = 8 for control and Doc+GPR77 Ab groups; n = 7 for Doc and Doc+IgG groups.

(B) Tumor size was monitored for the additional 8 weeks.

(C) The therapeutic responses were evaluated using the RECIST standard. $^{***}p < 0.001$ compared with the docetaxel treated group (−) by Fisher's exact test.

(D) Representative images of PDXs growth monitored by PET-CT. The circles indicate PDXs.

(E) Representative immunofluorescent images for TUNEL^{+} human-CK^{+} apoptotic tumor cells (upper row) and TUNEL^{+} human-α-SMA^{+} apoptotic human fibroblasts (lower row) in the harvested PDXs. Scale bars, 50 μm.

(F) Quantification of apoptotic human tumor cells and human fibroblasts in the harvested PDXs. n = 6 for each group.

(G) Fibroblasts and cancer cells were isolated from harvested PDXs. The proportions of CD10^{+}GPR77^{+} fibroblasts and ALDH1^{+} cancer cells were determined by flow cytometry. n = 5 for each group.

(F and G) Mean ± SEM, $^{***}p$ and $^{\#\#\#}p < 0.001$ compared with docetaxel treated group (−) by Student's t test.

(H) The signaling transduction pathways in CD10^{+} GPR77^{+} CAFs upon interacting with CSCs were illustrated.

tumor growth of the implanted PDXs (Figures 7B–7D). Furthermore, combined treatment with anti-GPR77 antibody dramatically enhanced apoptosis of both the tumor cells and the CAFs (Figure 7E and 7F). Moreover, administration of anti-GPR77 antibody significantly reduced the infiltration of CD10^{+}GPR77^{+} CAFs and the proportion of ALDH1^{+} breast CSCs in the PDXs (Figure 7G). Collectively, our data suggested that blocking GPR77 with neutralizing antibody promises an effective therapeutic strategy in suppressing breast tumorigenesis and enhancing chemotherapeutic effects.

DISCUSSION

CAFs can promote cancer progression by regulating CSCs and chemoresistance (Vermeulen et al., 2010). CAF-derived IL-6 is a key mediator for these effects, but it is only released by a proportion of CAFs in both breast (Rudnick et al., 2011) and pancreatic (Öhlund et al., 2017) cancers. Thus, therapeutic strategies by unselectively targeting whole CAF population are ineffective due to fibroblast heterogeneity and may even lead to cancer progression (Özdemir et al., 2014; Rhim et al., 2014). In this scenario, there is a pressing need to identify more specific and convenient markers to distinguish the IL-6-producing CAFs for precision treatment. Here, using transcriptomic profiling of clinical samples from breast cancer patients who received neoadjuvant chemotherapy and PDX tumors, we found that CD10 and GPR77, two surface proteins rarely associated with fibroblasts before, can define a human CAF subset that provides a survival niche for CSCs and protects them from chemotherapy-induced cell death. More importantly, the identified surface markers enable live-cell sorting, which is crucial to reveal mechanisms for the heterogeneous functions of the CAF subset. We found that the niches formed by CD10^{+}GPR77^{+} CAFs provide a constant source of paracrine IL-6 and IL-8 for the CSCs owing to persistent NF-κB signaling maintained by p65 phosphorylation and acetylation. Our study not only provides a molecular definition for the CSC-niche-forming CAF subset shared by various tumor types, but also highlights an efficient approach to acquire specific stromal cell subsets and to dissect their signaling pathways. Furthermore, our data showed that CD10^{+}GPR77^{+} CAFs form a protecting niche for CSCs under chemotherapeutic attack by enhancing the expression of

ABCG2 in cancer cells, which is a principal mechanism of CSC chemoresistance (Lou and Dean, 2007). More importantly, $CD10^+GPR77^+$ CAFs are not only the specific CAF subset responsible for inducing chemoresistance in cancer cells, but also are resistant to chemotherapy themselves by expressing a number of ABC transporters (data not shown). Thus, a more thorough understanding of the therapeutic response of tumor stromal cells is crucial to designing more effective treatment.

Maintenance of CSC phenotypes requires constant autocrine or paracrine signals in the niche (Plaks et al., 2015). Continuous NF-κB activation is frequently detected in cancer cells, and emerging evidence suggests that tumor stromal cells may also need sustained NF-κB activation to maintain their functions (Erez et al., 2010). Our data reveal that persistent NF-κB activation with sustained p65 nuclear retention in the $CD10^+GPR77^+$CAFs is essential to maintain their functions of paracrine IL6/IL8 secretion and providing survival niche for CSCs. Moreover, the prolonged NF-κB activation, herein, is not a result of continuous IKK or IκB phosphorylation but relies on post-translational modifications of p65, including phosphorylation and acetylation. This confirms a previous concept that the balance between import and export of nuclear p65 is finely tuned by its post-translational modifications (Chen et al., 2001). Thus, our current findings underscore the significance of p65 post-translational modifications in maintaining the inflammatory signals of CSC niche and the ensuing effects on sustaining paracrine cytokine secretion for CSCs.

More interestingly, our findings reveal that GPR77 is not only a surface marker for the CAF subset, but also serves as an essential signaling molecule that maintains p65 post-translational modification and sustains NF-κB activities in a positive feed-forward manner. A prerequisite for p65 acetylation at lysine 310 is its phosphorylation at serine 536, which can be a result of IKK or RSK1 activation (Chen and Greene, 2004). Here, we found that p65 phosphorylation at S536 is associated with high RSK1, but not IKK, activities in the $CD10^+GPR77^+$ CAFs, which can be completely abolished in vitro and in vivo by knocking down or neutralizing GPR77, a C5a receptor. It has been well appreciated that various complement mediators, including C5a, are abundant in different types of malignancies, which play an important role in tumor progression (Reis et al., 2018). Moreover, recent studies have demonstrated that both cancer cells and stromal cells can produce various complements, including C3a, C5a, and C5b-9, and further cleave them to bioactive forms via membrane-bound proteases (Afshar-Kharghan, 2017). More interestingly, several complement activators are transcribed by NF-κB, including Factor B (Huang et al., 2002) and Factor D (Su et al., 2015). Our present data extended these findings by showing that the autocrine C5a, whose production is controlled by NF-κB in the cancer-promoting CAF subset, helps to maintain GPR77-induced RSK-1 phosphorylation and sustain NF-κB activation. Although a variety of cytokines, such as CCL18 and IL-1β, in the tumor microenvironment may be responsible for initiating the NF-κB signaling by activating IKK in the CAF subset (Erez et al., 2010; Su et al., 2014), IKK activation is usually not sustainable due to numerous negative feedback loops (Perkins, 2012). This may account for the low IKK activities in the $CD10^+GPR77^+$CAFs, while NF-κB signaling is maintained by p65 protein phosphorylation and acetylation induced by its own transcribed GPR77 in a positive feed-forward manner. Hence, our findings highlight the role of the complement system in sustaining inflammation of tumor stromal cells and promoting cancer progression. A schema illustrating the positive feed-forward loop that underlies sustained NF-κB activation in the $CD10^+GPR77^+$CAFs is provided in the graphic abstract (Figure 7H). Herein, NF-κB signaling in the $CD10^+GPR77^+$CAFs, probably initiated by the inflammatory cytokines in the tumor milieu, enhances self-production of C5a, transcribes its receptor GPR77, and subsequently induces p65 phosphorylation via RSK1. As a result, the phosphorylated p65 is further acetylated by p300 and sustains its nuclear localization and NF-κB activation.

The identification of the $CD10^+GPR77^+$ CAF subset has a profound impact not only on predicting chemotherapeutic efficacy, but also on developing novel anti-tumor strategies. The prognostic values of CAFs, which were previously denoted by conventional markers such as α-SMA or FAP, are often different or even opposite in different studies (Paulsson and Micke, 2014). Indeed, the number of α-SMA^+/FAP^+ fibroblasts in the tumor stroma cannot predict chemotherapeutic response of breast cancer patients undergoing neo-adjuvant chemotherapy in our present study. On the other hand, though, $CD10^+GPR77^+$CAF abundance is closely associated with chemotherapeutic efficacy and patient survival in several cohorts of breast and lung cancer patients. Its prognostic value is particularly strong in ER^-HER2^- subtype and high-graded breast tumors, which is consistent with previous findings that breast cancer stem cells are more abundant in triple-negative and poorly differentiated breast cancer (Honeth et al., 2008). Thus, $CD10^+GPR77^+$CAFs infiltration may serve as a promising clinical biomarker to predict chemotherapy response and cancer patient outcome.

Ever since the discovery of CSCs in solid tumors, the field of cancer treatment is bursting with enthusiasm to target CSCs. However, specific markers to precisely identify CSCs in vivo are lacking in many tumor types, which poses a great hurdle to target these cells for therapeutic purposes (Kreso and Dick, 2014). Additionally, the eliminated CSCs may be replenished by non-CSCs in the presence of the supporting niche (Plaks et al., 2015), which may also undermine the therapeutic effects of directly targeting the CSCs. Nevertheless, targeting CSC niches may promise a more feasible therapeutic strategy than targeting CSC themselves. This assumption is corroborated by our findings that the $CD10^+GPR77^+$CAFs constitute a survival niche for CSCs in both breast and lung cancers, and targeting this CAF subset retards tumor formation and reverses chemoresistance by destroying the CSC niches. Furthermore, identifying the specific cell-surface marker that also functions as a most upstream signaling molecule greatly facilitates targeting the cancer-promoting CAF subset. In this context, our findings highlight the therapeutic potential of a neutralizing monoclonal antibody against GPR77, as it successfully eradicates the $CD10^+GPR77^+$CAFs and CSCs and thus significantly suppresses tumor formation and improves chemotherapy efficacy in PDX-bearing mice. Furthermore, given that no single marker is exclusively expressed by a single cell subset, whether targeting both CD10 and GPR77 may represent a more precise therapy

to eliminate CSC niches and suppress tumor progression warrants further investigation.

STAR★METHODS

Detailed methods are provided in the online version of this paper and include the following:

- KEY RESOURCES TABLE
- CONTACT FOR REAGENT AND RESOURCE SHARING
- EXPERIMENTAL MODEL AND SUBJECT DETAILS
  - Patients and Tissue Samples
  - Primary Cell Culture
  - Co-injection Animal Experiments
  - Patient Derived Xenograft (PDX) Experiments
- METHOD DETAILS
  - Fluorescence-Activated Cell Sorting
  - Co-Culture Experiments
  - Flow Cytometry
  - Apoptosis Analysis
  - TUNEL Assay
  - Gene Microarrays
  - Immunofluorescence
  - Immunohistochemistry
  - Cytokine Antibody Arrays
  - ELISA
  - Western Blot
  - qRT-PCR
  - MTT Assay
  - Sphere Formation Assay
  - Luciferase Reporter Assay
  - Immunoprecipitation
  - Chromatin Immunoprecipitation Assay (ChIP)
  - Osteogenesis
  - Adipogenesis
  - PET/CT Imaging
- QUANTIFICATION AND STATISTICAL ANALYSIS
- DATA AND SOFTWARE AVAILABILITY

SUPPLEMENTAL INFORMATION

Supplemental Information includes four tables and seven figures and can be found with this article online at https://doi.org/10.1016/j.cell.2018.01.009.

ACKNOWLEDGMENTS

This work was supported by grants from the National Key Research and Development Program of China (2017YFA0106300 and 2016YFC1302300), the National Natural Science Foundation of China (81622036,81472468, 81672614, 81720108029, 81621004, 81490750, 81230060, 81442009, 81372819, 81572596, U1601223, and 81672620), Science Foundation of Guangdong Province (2016A030306023, 2014A030313094, S2012030006287, 2016B030229004, 2015B050501004, 2017A030313878, and 2017A030313828), Tip-top Scientific and Technical Innovative Youth Talents of Guangdong special support program (No. 2016TQ03R553), Guangzhou science and technology project (201710010083 and 2014J4100170, 201704020131), Guangzhou Science Technology and Innovation Commission (201508020008 and 201508020249), Guangdong Science and Technology Department (2015B050501004), Translational medicine public platform of Guangdong Province (4202037), and Guangdong Department of Science & Technology Translational Medicine Center grant (2011A080300002).

AUTHOR CONTRIBUTIONS

S.S., J.C., H.Y., Q.L., and E.S. conceived the ideas and designed the experiments. S.S, J.C., D.H., J.L., F.C., L.Y., and D.L. performed the experiments. H.Y., F.S., and E.S. performed neo-adjuvant chemotherapy and clinical data analysis. S.S., J.C., D.H., J.L., F.C., and L.Y. analyzed the data. S.S., J.C., X.C., and E.S. wrote the paper.

DECLARATION OF INTERESTS

The authors declare no competing interests.

Received: October 10, 2017
Revised: December 28, 2017
Accepted: January 4, 2018
Published: January 25, 2018

REFERENCES

Afshar-Kharghan, V. (2017). The role of the complement system in cancer. J. Clin. Invest. *127*, 780–789.

Amakye, D., Jagani, Z., and Dorsch, M. (2013). Unraveling the therapeutic potential of the Hedgehog pathway in cancer. Nat. Med. *19*, 1410–1422.

Byrne, A.T., Alférez, D.G., Amant, F., Annibali, D., Arribas, J., Biankin, A.V., Bruna, A., Budinská, E., Caldas, C., Chang, D.K., et al. (2017). Interrogating open issues in cancer precision medicine with patient-derived xenografts. Nat. Rev. Cancer *17*, 254–268.

Chen, L.F., and Greene, W.C. (2004). Shaping the nuclear action of NF-kappaB. Nat. Rev. Mol. Cell Biol. *5*, 392–401.

Chen, L.F., Fischle, W., Verdin, E., and Greene, W.C. (2001). Duration of nuclear NF-kappaB action regulated by reversible acetylation. Science *293*, 1653–1657.

Covas, D.T., Panepucci, R.A., Fontes, A.M., Silva, W.A., Jr., Orellana, M.D., Freitas, M.C., Neder, L., Santos, A.R., Peres, L.C., Jamur, M.C., and Zago, M.A. (2008). Multipotent mesenchymal stromal cells obtained from diverse human tissues share functional properties and gene-expression profile with CD146+ perivascular cells and fibroblasts. Exp. Hematol. *36*, 642–654.

Erez, N., Truitt, M., Olson, P., Arron, S.T., and Hanahan, D. (2010). Cancer-Associated Fibroblasts Are Activated in Incipient Neoplasia to Orchestrate Tumor-Promoting Inflammation in an NF-kappaB-Dependent Manner. Cancer Cell *17*, 135–147.

Honeth, G., Bendahl, P.O., Ringnér, M., Saal, L.H., Gruvberger-Saal, S.K., Lövgren, K., Grabau, D., Fernö, M., Borg, A., and Hegardt, C. (2008). The CD44+/CD24- phenotype is enriched in basal-like breast tumors. Breast Cancer Res. *10*, R53.

Huang, Y., Krein, P.M., Muruve, D.A., and Winston, B.W. (2002). Complement factor B gene regulation: synergistic effects of TNF-alpha and IFN-gamma in macrophages. J. Immunol. *169*, 2627–2635.

Kalluri, R. (2016). The biology and function of fibroblasts in cancer. Nat. Rev. Cancer *16*, 582–598.

Karnoub, A.E., Dash, A.B., Vo, A.P., Sullivan, A., Brooks, M.W., Bell, G.W., Richardson, A.L., Polyak, K., Tubo, R., and Weinberg, R.A. (2007). Mesenchymal stem cells within tumour stroma promote breast cancer metastasis. Nature *449*, 557–563.

Korkaya, H., Liu, S., and Wicha, M.S. (2011). Breast cancer stem cells, cytokine networks, and the tumor microenvironment. J. Clin. Invest. *121*, 3804–3809.

Korkaya, H., Kim, G.I., Davis, A., Malik, F., Henry, N.L., Ithimakin, S., Quraishi, A.A., Tawakkol, N., D'Angelo, R., Paulson, A.K., et al. (2012). Activation of an IL6 inflammatory loop mediates trastuzumab resistance in HER2+ breast cancer by expanding the cancer stem cell population. Mol. Cell *47*, 570–584.

Kreso, A., and Dick, J.E. (2014). Evolution of the cancer stem cell model. Cell Stem Cell *14*, 275–291.

Lou, H., and Dean, M. (2007). Targeted therapy for cancer stem cells: the patched pathway and ABC transporters. Oncogene *26*, 1357–1360.

Meads, M.B., Gatenby, R.A., and Dalton, W.S. (2009). Environment-mediated drug resistance: a major contributor to minimal residual disease. Nat. Rev. Cancer *9*, 665–674.

Öhlund, D., Handly-Santana, A., Biffi, G., Elyada, E., Almeida, A.S., Ponz-Sarvise, M., Corbo, V., Oni, T.E., Hearn, S.A., Lee, E.J., et al. (2017). Distinct populations of inflammatory fibroblasts and myofibroblasts in pancreatic cancer. J. Exp. Med. *214*, 579–596.

Orimo, A., and Weinberg, R.A. (2006). Stromal fibroblasts in cancer: a novel tumor-promoting cell type. Cell Cycle *5*, 1597–1601.

Orimo, A., Gupta, P.B., Sgroi, D.C., Arenzana-Seisdedos, F., Delaunay, T., Naeem, R., Carey, V.J., Richardson, A.L., and Weinberg, R.A. (2005). Stromal fibroblasts present in invasive human breast carcinomas promote tumor growth and angiogenesis through elevated SDF-1/CXCL12 secretion. Cell *121*, 335–348.

Oskarsson, T., Batlle, E., and Massagué, J. (2014). Metastatic stem cells: sources, niches, and vital pathways. Cell Stem Cell *14*, 306–321.

Özdemir, B.C., Pentcheva-Hoang, T., Carstens, J.L., Zheng, X., Wu, C.C., Simpson, T.R., Laklai, H., Sugimoto, H., Kahlert, C., Novitskiy, S.V., et al. (2014). Depletion of carcinoma-associated fibroblasts and fibrosis induces immunosuppression and accelerates pancreas cancer with reduced survival. Cancer Cell *25*, 719–734.

Paulsson, J., and Micke, P. (2014). Prognostic relevance of cancer-associated fibroblasts in human cancer. Semin. Cancer Biol. *25*, 61–68.

Perkins, N.D. (2012). The diverse and complex roles of NF-κB subunits in cancer. Nat. Rev. Cancer *12*, 121–132.

Plaks, V., Kong, N., and Werb, Z. (2015). The cancer stem cell niche: how essential is the niche in regulating stemness of tumor cells? Cell Stem Cell *16*, 225–238.

Prowell, T.M., and Pazdur, R. (2012). Pathological complete response and accelerated drug approval in early breast cancer. N. Engl. J. Med. *366*, 2438–2441.

Reis, E.S., Mastellos, D.C., Ricklin, D., Mantovani, A., and Lambris, J.D. (2018). Complement in cancer: untangling an intricate relationship. Nat. Rev. Immunol. *18*, 5–18.

Rhim, A.D., Oberstein, P.E., Thomas, D.H., Mirek, E.T., Palermo, C.F., Sastra, S.A., Dekleva, E.N., Saunders, T., Becerra, C.P., Tattersall, I.W., et al. (2014). Stromal elements act to restrain, rather than support, pancreatic ductal adenocarcinoma. Cancer Cell *25*, 735–747.

Rittirsch, D., Flierl, M.A., Nadeau, B.A., Day, D.E., Huber-Lang, M., Mackay, C.R., Zetoune, F.S., Gerard, N.P., Cianflone, K., Köhl, J., et al. (2008). Functional roles for C5a receptors in sepsis. Nat. Med. *14*, 551–557.

Rudnick, J.A., Arendt, L.M., Klebba, I., Hinds, J.W., Iyer, V., Gupta, P.B., Naber, S.P., and Kuperwasser, C. (2011). Functional heterogeneity of breast fibroblasts is defined by a prostaglandin secretory phenotype that promotes expansion of cancer-stem like cells. PLoS ONE *6*, e24605.

Su, S., Liu, Q., Chen, J., Chen, J., Chen, F., He, C., Huang, D., Wu, W., Lin, L., Huang, W., et al. (2014). A positive feedback loop between mesenchymal-like cancer cells and macrophages is essential to breast cancer metastasis. Cancer Cell *25*, 605–620.

Su, X., Yan, H., Huang, Y., Yun, H., Zeng, B., Wang, E., Liu, Y., Zhang, Y., Liu, F., Che, Y., et al. (2015). Expression of FABP4, adipsin and adiponectin in Paneth cells is modulated by gut Lactobacillus. Sci. Rep. *5*, 18588.

Sugimoto, H., Mundel, T.M., Kieran, M.W., and Kalluri, R. (2006). Identification of fibroblast heterogeneity in the tumor microenvironment. Cancer Biol. Ther. *5*, 1640–1646.

Takahashi, R.U., Miyazaki, H., Takeshita, F., Yamamoto, Y., Minoura, K., Ono, M., Kodaira, M., Tamura, K., Mori, M., and Ochiya, T. (2015). Loss of microRNA-27b contributes to breast cancer stem cell generation by activating ENPP1. Nat. Commun. *6*, 7318.

Vermeulen, L., De Sousa E Melo, F., van der Heijden, M., Cameron, K., de Jong, J.H., Borovski, T., Tuynman, J.B., Todaro, M., Merz, C., Rodermond, H., et al. (2010). Wnt activity defines colon cancer stem cells and is regulated by the microenvironment. Nat. Cell Biol. *12*, 468–476.

Yu, F., Yao, H., Zhu, P., Zhang, X., Pan, Q., Gong, C., Huang, Y., Hu, X., Su, F., Lieberman, J., and Song, E. (2007). let-7 regulates self renewal and tumorigenicity of breast cancer cells. Cell *131*, 1109–1123.

STAR★METHODS

KEY RESOURCES TABLE

REAGENT or RESOURCE	SOURCE	IDENTIFIER
Antibodies		
PE mouse anti-human EpCAM	eBioscience	Cat# 12-9326; RRID: AB_837110
APC mouse anti-human CD31	eBioscience	Cat# 17-0319; RRID: AB_10853188
FITC mouse anti-human CD45	eBioscience	Cat# 11-9459; RRID: AB_1907395
APC mouse anti-human CD10	eBioscience	Cat# 17-0106-42; RRID: AB_11043552
PE mouse anti-human GPR77	BioLegend	Cat# 342404; RRID: AB_2247831
FITC mouse anti-human CD44	BD Biosciences	Cat# 555478; RRID: AB_395870
PE mouse anti-human CD24	BD Biosciences	Cat# 555428; RRID: AB_395822
Goat anti-human α-SMA	Abcam	Cat# ab21027; RRID: AB_1951138
Goat anti-human ALDH1	R&D	Cat# AF5869; RRID: AB_2044597
Rabbit anti-human CD10	Abcam	Cat# ab73409; RRID: AB_10859232
Mouse anti-human GPR77	BioLegend	Cat# 342402; RRID: AB_2113254
Rabbit anti-human Numb	Abcam	Cat# ab14140; RRID: AB_443023
Rabbit anti-human p65	CST	Cat# 8242; RRID: AB_10859369
Rabbit anti-human ac-p65	Abcam	Cat# ab19870; RRID: AB_776753
Rabbit anti-human phospho-p65(Ser536)	CST	Cat# 3033; RRID: AB_331284
Rabbit anti-human melthy-p65	CST	Cat# 13188
Mouse anti-human α-SMA	R&D	Cat# MAB1420; RRID: AB_262054
Rabbit anti-human Collagen I	Abcam	Cat# ab34710; RRID: AB_731684
Rabbit anti-human Ki-67	CST	Cat# 9027; RRID: AB_2636984
Rabbit anti-human Collagen III	Abcam	Cat# ab7778; RRID: AB_306066
Rabbit anti-human Caspase-3	CST	Cat# 9662; RRID: AB_331439
Rabbit anti-human Cleaved caspase-3	CST	Cat# 9664; RRID: AB_2070042
Rabbit anti-human PARP	CST	Cat# 9532; RRID: AB_659884
Rabbit anti-human Cleaved PARP	CST	Cat# 5625; RRID: AB_10699459
Rabbit anti-human phospho-RSK1(Ser380)	CST	Cat# 9335; RRID: AB_561151
Rabbit anti-human RSK1	CST	Cat# 8408; RRID: AB_10828594
Goat anti-human p300	R&D	Cat# AF3789; RRID: AB_2098107
HRP Mouse anti-human GAPDH	Proteintech	Cat# HRP-60004; RRID: AB_2107436
Neutralizing Rat anti-human IL-6	BD Biosciences	Cat# 554543; RRID: AB_398568
Neutralizing Mouse anti-human IL-8	BD Biosciences	Cat# 554726; RRID: AB_395531
Neutralizing Mouse anti-human GRO	R&D	Cat#MAB276; RRID: AB_2087567
Neutralizing Mouse anti-human M-CSF	R&D	Cat#MAB216; RRID: AB_2085064
Neutralizing Mouse anti-human IL-10	R&D	Cat#MAB2173; RRID: AB_1674226
Neutralizing Mouse anti-human GPR77	Abcam	Cat# Ab77982; RRID: AB_1566236
Neutralizing Mouse anti-human C5a	R&D	Cat# MAB 2037; RRID: AB_2067045
Rabbit IgG	CST	Cat# 3900; RRID: AB_1550038
Bacterial and Virus Strains		
LV3 lentiviral vector	Genepharma,Shanghai	N/A

(*Continued on next page*)

Continued

REAGENT or RESOURCE	SOURCE	IDENTIFIER
Biological Samples		
Paraffin breast cancer sections	Sun Yat-sen Memorial Hospital, Sun Yat-sen University; The First Affiliated Hospital, Shantou University Medical College	N/A
Paraffin Lung cancer sections	Sun Yat-sen Memorial Hospital, Sun Yat-sen University	N/A
Fresh breast cancer samples and lung cancer samples (used for isolation of fibroblasts or PDX experiments)	Sun Yat-sen Memorial Hospital, Sun Yat-sen University	Related to Table S2
Chemicals, Peptides, and Recombinant Proteins		
Dynabeads® Protein A	Life	Cat# 10001D
bFGF	Peprotech	Cat# 100-18B
Dexamethasone	Sigma	Cat# D4902
Vitamin C	Sigma	Cat# 856061
Glycerophosphate	Sigma	Cat# 9422
Alizarin red S	Sigma	Cat# A5533
Indomethacin	Sigma	Cat# I7378
Isobutylmethylxanthine	Sigma	Cat# I7018
Insulin	Sigma	Cat# I3536
Oil-red-O powder	Sigma	Cat# O0625
JSH-23	Selleck	Cat#S7351
Sc-3060	Santa Cruz	Cat#Sc-3060
C646	Selleck	Cat#S7152
Anacardic Acid	Selleck	Cat#S7582
Bay11-7082	Selleck	Cat#S2913
BMS-345541	Selleck	Cat#S8044
Critical Commercial Assays		
anti-Fibroblast MicroBeads	Miltenyi Biotec	Cat# 130-050-601
Tumor Cell Enrichment and Detection Kit	Miltenyi Biotec	Cat# 130-090-500
ALDEFLUOR kit	Stem Cell Technologies	Cat# 01700
Annexin V Apoptosis Detection Kit	eBioscience	Cat# 88-8005-74
In Situ Cell Death Detection Kit, POD	Roche	Cat# 11684817910
EZ-Magna ChIP Chromatin Immunoprecipitation kit	Millipore, Billerica, MA	Cat# 17-408
IL-6 ELISA Kit	eBioscience	Cat# 88-7066-86
IL-8 ELISA Kit	eBioscience	Cat# 88-8086-86
IL-10 ELISA Kit	eBioscience	Cat# 88-7106-86
M-CSF ELISA Kit	eBioscience	Cat# ELH-MCSF
GRO ELISA kit	RayBiotech	Cat# ELH-GRO
Deposited Data		
Gene microarray data (Raw and analyzed data)	This paper	GEO:GSE108565
Experimental Models: Cell Lines		
MCF-7	ATCC	HTB-22
SK-BR3	ATCC	HTB-30
BT-549	ATCC	HTB-122D
A549	ATCC	CRM-CCL-185
NCI-H1299	ATCC	CRL-5803

(*Continued on next page*)

Continued

REAGENT or RESOURCE	SOURCE	IDENTIFIER
Experimental Models: Organisms/Strains		
N/A		
Oligonucleotides		
qRT-PCR primers, see Table S3	This paper	N/A
ChIP primers, see Table S3	This paper	N/A
shRNA targeting sequences, see Table S4	This paper	N/A
Recombinant DNA		
N/A		
Software and Algorithms		
ImageJ	NIH	https://imagej.nih.gov/ij/
Prism 5.0	GraphPad Software	http://www.graphpad.com/
FlowJo	N/A	https://www.flowjo.com/
X-tile	N/A	N/A
SPSS	N/A	http://www.spss.com.cn/
Primer premier	N/A	http://www.premierbiosoft.com/primerdesign/
Imaris 9.0 Microscopy Image Analysis Software	N/A	N/A

CONTACT FOR REAGENT AND RESOURCE SHARING

Further information and requests for resources and reagents should be directed to and will be fulfilled by the Lead Contact, Erwei Song (songew@mail.sysu.edu.cn).

EXPERIMENTAL MODEL AND SUBJECT DETAILS

Patients and Tissue Samples

Tumor samples were obtained from 578 patients with invasive breast carcinoma who underwent neoadjuvant therapy at the Sun Yat-Sen Memorial Hospital, Sun Yat-Sen University (Guangzhou, China) between 2006 and 2015. Patients received neoadjuvant chemotherapy regimens of AC (doxorubicin 60 mg/m^2 and cyclophosphamide 600 mg/m^2) every 3 weeks for 4 cycles, followed by paclitaxel (80 mg/m^2) weekly for 12 weeks, or TC (Docetaxel 75 mg/m^2 and cyclophosphamide 600 mg/m^2) every 3 weeks for 4 cycles. Her2-positive patients were treated with concomitant trastuzumab (initial loading dose of 4mg/kg and subsequent doses of 2 mg/kg/wk) weekly. Therapeutic effects were evaluated according to the standard of RECIST (Response Evaluation Criteria in Solid Tumors). Complete Response (CR) was defined as disappearance of all lesions in both primary tumor and lymph nodes; Partial Response (PR) was defined as at least a 30% reduction in the sum of the longest diameter of target lesions; Progressive Disease (PD) was defined as at least a 20% increase in the sum of the longest diameter of target lesions; and Stable Disease (SD) was defined as neither sufficient shrinkage to qualify as PR nor sufficient increase to qualify as PD. CR and PR were classified as chemosensitive, while SD and PD were classified as chemoresistant. Additionally, 613 chemotherapy-naive invasive breast carcinoma samples from Sun Yat-Sen Memorial Hospital, Sun Yat-Sen University (Guangzhou, China) were used for kaplan-meier survival analysis and tumor samples of 206 patients with invasive breast carcinoma were collected from the First Affiliated Hospital, Shantou University Medical College (Shantou, China) for breast cancer external validation. Moreover, tumor samples of 256 patients with NSCLC were collected from Sun Yat-Sen Memorial Hospital. All samples were collected from patients with informed consent, and all related procedures were performed with the approval of the internal review and ethics boards of the indicated hospitals.

Primary Cell Culture

Primary cancer associated fibroblasts (CAFs) and breast cancer cells were isolated from invasive ductal carcinoma samples obtained from vacuum-assisted biopsies or surgery. Normal breast fibroblasts (NBFs) were obtained from reduction mammaplasties. Briefly, tissues were digested by collagenase type I, collagenase type III and hyaluronidase (1.5 mg/ml, Sigma Aldrich) at 37°C with agitation for 2-3 hr in DMEM with 10% FBS. Thereafter, in order to isolate primary fibroblasts, the dissociated tissues were incubated without shaking for 5 min at room temperature, followed by the separation of stromal cell-enriched supernatant to a new tube. The stromal fraction was collected by centrifuge at 250 g for 5 min (Orimo et al., 2005). In some experiments, to acquire purer fibroblast populations, we employed magnetic-activated cell sorting (MASC) with anti-FSP (fibroblast specific protein) to purify the primary fibroblasts isolated as indicated above. On the other hand, the primary cancer cells were purified by MACS with CD326 (EpCAM)

Tumor Cell Enrichment and Detection Kit according to the manufacturer's instructions. Human fibroblasts were then cultured in DMEM with 10% FBS and the purity of fibroblasts was validated by flow cytometry analysis and immunofluorescent staining, which showed that primary CAFs were negative for EpCAM, CD31 and CD45 and positive for α-SMA and FAP (> 95%). The first to fifth passages of primary fibroblasts were used in our experiments. Primary breast cancer cells were cultured in DMEM with 20% FBS. The BMSCs were isolated from bone marrow of healthy donors. Briefly, to isolate the bone marrow-derived MSCs, 10mL BM aspirates obtained from healthy volunteer were diluted 1:1 with L-DMEM and layered over Ficoll-Paque solution (Amersham Biosciences). After centrifugation at 800 g for 20 min, mononuclear cells were collected from the interface, washed and resuspended in human MSC growth media (L-DMEM with 10%FBS and 10ng/ml bFGF (Cat.No#100-18B, Peprotech). After 3 days, the non-adherent cells were removed by replacing with fresh medium. Adherent cells were further cultured with media changed every 3 days and passaged at a ratio of 1:3 when they were 70%–80% confluent. Second- or third-passage of MSCs were used for individual experiments. The clinical features of patients whose tumors were used for CAF isolation were provided in Table S2. All samples were collected from the donors with informed consent, and all related procedures were performed with the approval of the Internal Review and Ethics Boards of Sun Yat-Sen Memorial Hospital.

To knock down specific target genes, 1×10^6 cells were transduced with the LV3 lentivirus carrying shRNA constructs (multiplicity of infection[MOI] of 100) overnight at 37°C with 5 μg/ml protamine sulfate (Sigma). Lentivirus packaging was provided by GenePharma Inc (Shanghai, China). The targeting sequences of each shRNA are listed in Table S4. To inhibit specific signaling pathways, CAFs were pretreated with vehicle (DMSO), 6 μM JSH-23, 10 μM Sc-3060, 20 μM C646, 10 μM Anacardic Acid, 2 μM Bay11-7082 and 10 μM BMS-345541 for 1 hr at 37°C prior to the experiments.

Co-injection Animal Experiments

Tumorigenesis

For the first generation of xenografts, serial concentration of MCF-7 cells or primary breast cancer cells mixed with various subsets of CAFs were co-injected into the mammary fat-pads of 6-week-old NOD/SCID mice at 1:3 ratio as previously described (Orimo et al., 2005). To provide estrogen for MCF-7 tumor growth, each mouse was implanted with a 1.7 mg 17β-estradiol pellet (60-day release, Innovative Research of America, Sarasota, FL, USA) 3 days before inoculation of MCF-7 cells. Tumor formation was assessed for up to 2 months and the xenografts were harvested for subsequent transplantation. The xenografts were dissociated by collagenase type I (1.5 mg/ml) and collagenase type III (1.5 mg/ml) at 37°C with agitation for half an hour in DMEM with 10% FBS. Single cell suspensions were obtained by filtration through a 40 μm filter and the breast cancer cells were isolated and purified using CD326 (EpCAM) Tumor Cell Enrichment and Detection Kit according to the manufacturer's instructions. Then, purified breast cancer cells were transplanted into the fat-pads of a new batch of 6-weeks-old NOD/SCID mice without fibroblasts. Tumor formation was observed for the following 2 months.

Chemoresistance

$1x10^6$ MCF-7 cells alone or mixed with various subsets of CAFs at a ratio of 1:3 were implanted into the fat-pads of 6-weeks-old NOD/SCID mice. Docetaxel administration was started at a dose of 10 mg/kg i.p. once per week when the tumors reached approximately 3mm in diameter. After 6 weeks of treatment, the xenografts were harvested, fixed in 10% formalin and embedded in paraffin for subsequent analysis. Tumor size was measured every week with a caliper, and the volume was calculated using the standard modified formula Volume (mm^3) = (length × $height^2$)/2. All mice used in this project were maintained under defined conditions at the Animal Experiment Center of Sun Yat-Sen University, and all animal experiments were approved by the Animal Care and Use Committee of Sun Yat-Sen University.

Patient Derived Xenograft (PDX) Experiments

To establish patient-derived xenografts, primary tumor specimens were collected from breast cancer patients who underwent tumor resection at Sun Yat-Sen Memorial Hospital, Sun Yat-Sen University (Guangzhou, China) between 2016 and 2017. The clinical features of patients were provided in Table S2. Eight-week-old NOD-SCID mice under pathogen-free conditions were used for patient-derived xenograft transplantation. Briefly, a small incision was made on the abdomen of anaesthetized NOD-SCID mice to reveal the mammary gland and primary breast tumor samples were minced into 1 mm^3 sized fragments and injected directly into the fourth pair of mammary fat pads. The incision was then closed up with sutures. The time from cancer samples collection to mouse implantation ranges from 30-180 min. The tumor formation was monitored in the next three months since implantation.

Tumorigenesis

In some experiments, neutralizing antibodies against IL-6 (2mg/kg), IL-8 (2mg/kg) or GPR77 (0.5mg/kg) were administrated concomitantly via tail vein when the breast cancer fragments were implanted into the fat pads of NOD-SCID mice and repeated every three days. And the tumor formation was monitored for indicated time since implantation.

Chemoresistance

The combined treatment of neutralizing antibodies and chemotherapy was performed when the longest diameter of xenografts reached 5mm. Neutralizing antibodies against IL-6 (2mg/kg), IL-8 (2mg/kg) or GPR77 (0.5mg/kg) were administrated via tail vein every three days and docetaxel (10mg/kg) were injected by intraperitoneal injection per week. The therapeutic responses were assessed refer to the human clinical evaluation standard, RECIST (Response Evaluation Criteria in Solid Tumors). Complete Response (CR) was defined as disappearance of tumor; Partial Response (PR) was defined as at least a 30% reduction in the sum of the longest

diameter of target lesions; Progressive Disease (PD) was defined as at least a 20% increase in the sum of the longest diameter of target lesions; and Stable Disease (SD) was defined as neither sufficient shrinkage to qualify as PR nor sufficient increase to qualify as PD. CR and PR were classified as chemosensitive, while SD and PD were classified as chemoresistant.

METHOD DETAILS

Fluorescence-Activated Cell Sorting

Different subsets of CAFs ($CD10^+GPR77^+$ CAFs and $CD10^+GPR77^+$-depleted CAFs) were selected by flow cytometric cell sorting (FACS). The FACS was performed on single cell suspensions using flow cytometer (BD Influx). Before cell sorting, primary CAFs were resuspended in PBS containing 1% FBS and incubated with antibodies against CD10 and GPR77 for 30min at 4°C. The purity of the sorted populations was verified by flow cytometry.

Co-Culture Experiments

MCF-7, SK-BR3 and BT-549 breast cancer cells as well as A549 and NCI-H1299 lung cancer cells were obtained from American Type Culture Collection (ATCC) and cultured according to standard protocols. Co-culture experiments were performed by seeding breast cancer cells ($1x10^5$) in the lower chamber and fibroblasts ($1x10^5$) in the upper chamber of a 6-well transwell apparatus with 0.4um pore size (Corning Incorporated, NY, USA). The co-cultured cells were passaged once they grew to 90% of confluence and were subjected to further analysis after 2 weeks of co-culture.

Flow Cytometry

For cell surface marker analysis, cells were resuspended in PBS containing 1% FBS and stained with fluorescent-conjugated antibodies against CD10, GPR77, CD44, CD24 for 30min at 4°C. For the detection of ALDH1 activity, ALDEFLUOR kit was used according to the manufacturer's instructions. Specimens were subsequently analyzed by BD Accuri C6 Flow cytometer.

Apoptosis Analysis

Cells treated with indicated chemotherapeutic agents for indicated time were dissociated by 0.25% trypsin-EDTA and harvested by centrifugation. Apoptosis was determined using Annexin V Apoptosis Detection Kit. Briefly, cells were incubated with 100 μL of binding buffer containing 5 μL of FITC-conjugated Annexin V antibody for 15min at room temperature. After incubation, cells were washed and resuspended in binding buffer (200 μl) containing 5 μL of Propidium Iodide Staining Solution and analyzed by flow cytometry immediately.

TUNEL Assay

For TUNEL assay, the slides were stained using the In Situ Cell Death Detection Kit, POD at 37°C for 30 min, followed by incubation with Alexa Fluor-conjugated secondary antibodies (Invitrogen) for 1 hr at room temperature. DAPI was then used for counterstaining of the nuclei and images were obtained by laser scanning confocal microscopy (LSM780, Zeiss).

Gene Microarrays

mRNA microarray analysis was performed with 15 μg of total RNA using the Human 12 × 135K Gene Expression Array (Roche NimbleGen). The data were analyzed using an Axon GenePix 4000B scanner (Molecular Devices Corporation) piloted by GenePix Pro 6.0 software (Axon). Scanned images were then imported into NimbleScan software (version 2.5) for grid alignment and expression data analysis. Expression data were normalized through quantile normalization, and the Robust Multichip Average (RMA) algorithm was included in the NimbleScan software. The microarray data were deposited in the public database. For gene set enrichment analysis (GSEA), normalized expression data were analyzed and visualized with the GSEA software (version 2.2.0, http://www.broadinstitute.org/gsea). The normalized enrichment score (NES) and false discovery rate (FDR) were calculated for comparison.

Immunofluorescence

Paraffin-embedded samples were sectioned at 4 μm thickness. Antigen retrieval was performed by a pressure cooker for 15-20min in 0.01M citrate buffer (pH 6.0) to remove aldehyde links formed during initial fixation of tissues. Then, sections were blocked in PBS containing 10% donkey serum or 2% bovine serum albumin for 1hr at room temperature. Cells for immunofluorescence were fixed with 4% paraformaldehyde for 15min at room temperature, washed with PBS and permeabilized with 0.2% Triton X-100 in PBS for 15min. Thereafter, cells were blocked in PBS with 2% BSA for 1 hr at room temperature. After blocking, samples were incubated with primary antibodies specific for goat-anti-human α-SMA (1:100), mouse-anti-human ALDH1 (1:100), rabbit-anti-human CD10 (1:30), mouse-anti-human GPR77 (1:30), rabbit-anti-human Numb (1:50), rabbit-anti-human p65 (1:50), or rabbit-anti-human ac-p65 (1:50) overnight at 4°C. Incubation of Alexa Fluor-conjugated secondary antibodies (Invitrogen) was carried out for 1 hr at room temperature. DAPI was then used for counterstaining the nuclei and images were obtained by laser scanning confocal microscopy (LSM780, Zeiss). The quantification of the proportion of $CD10^+GPR77^+$ CAFs in clinical samples was determined by co-expressing analysis of

CD10 and GPR77 in α-SMA positive cells using Imaris 9.0 Microscopy Image Analysis Software. Two cases in Figure S1H represented the analysis method. The percentage of $CD10^{+}GPR77^{+}$ CAFs equal to co-locating area of CD10 and GPR77 divided by α-SMA positive area.

Immunohistochemistry

Paraffin-embedded samples were sectioned at 4 μm thickness. Antigen retrieval was performed by a pressure cooker for 15-20min in 0.01M citrate buffer (pH 6.0) to remove aldehyde links formed during initial fixation of tissues. Specimens were incubated with antibodies specific for α-SMA (1:100), Collagen I (1:100), ALDH1 (1:100), or Ki-67 (1:100) overnight at 4°C and the immunodetection was performed on the following day using DAB (Dako) according to the manufacturer's instructions.

Cytokine Antibody Arrays

Human Cytokine Antibody Arrays V kit (Raybiotech) was used according to the manufacturer's instructions. Briefly, the arrays were blocked, incubated with 100 μL of condition medium overnight, followed by biotin-conjugated antibodies (1/250) incubation for 2 hr and with HRP-linked secondary antibody (1/1000) for 1 hr. The membranes were incubated with chemiluminescent substrate and exposed to X-ray film for 15min before development. Quantitative array analysis was performed using Array Vision Evaluation 8.0 (GE Healthcare Life Science).

ELISA

Primary fibroblasts were cultured in DMEM with 10% human serum until 80% of confluency. The cells were then washed with PBS and cultured in fresh serum-free media. Supernatants were harvested 24hr later and used for subsequent ELISA assay. The IL-6, IL-8, IL-10, and M-CSF ELISA kits were purchased from eBioscience and the GRO ELISA kit was purchased from RayBiotech. All experiments were performed according to the manufacturer's instructions.

Western Blot

Protein was extracted from the cells using RIPA buffer, resolved by SDS–polyacrylamide gels and then transferred to PVDF membranes. Primary antibodies against α-SMA (Cat.No. MAB1420, R&D; 1:1000), FAP (1:500), collagen I (1:5000), collagen III (1:5000), caspase-3 (1:1000), cleaved caspase-3 (1:1000), PARP (1:1000), cleaved PARP (1:1000), p65 (1:1000), ac-p65 (1:500), methyl-p65 (1:1000), stat3(1:1000), phospho-stat3 (1:1000), p300 (1:500), and GAPDH (1:10,000) were used. Peroxidase conjugated secondary antibody (CST) was used and the antigen-antibody reaction was visualized by enhanced chemiluminescence assay (ECL, Thermo).

qRT-PCR

Quantitative reverse transcription PCR (qRT-PCR) was performed using SYBR Premix Ex Taq kit (TaKaRa, Japan) according to the manufacturer's instruction. The primer sequences were listed in Table S3. Data were collected and analyzed with a LightCycler 480 instrument (Roche).

MTT Assay

3–(4,5-dimethylthiazol-2-yl)22,5-diphenyltetrazolium bromide (MTT, Sigma) assay was used to determine viability of the indicated cells. Briefly, 1000 cells were seeded onto 96-well plates and incubated overnight at 37°C. The cells were then treated with indicated chemotherapeutic agents. Thereafter, MTT solution was added to each individual well, and the plates were incubated for 4 hr at 37°C. Then the media was removed and 150 μL DMSO was added to dissolve the formazan crystals. The absorbance was measured at 540nm by Infinite F500 (Tecan). Six replicate wells were included in each analysis and at least three independent experiments were conducted.

Sphere Formation Assay

Cancer cells (1000 cells/ml) were cultured in ultra-low adhesion plates (Corning) in serum-free DMEM-F12 (GIBCO), containing B27 (1:50, Invitrogen), 20 ng/mL EGF (BD Biosciences), 0.4% bovine serum albumin (Sigma), and 4 mg/ml insulin (Sigma). After culturing for 10 days, mammospheres with diameter > 75μm were counted. Six replicate wells were included in each analysis and at least three independent experiments were conducted.

Luciferase Reporter Assay

pNF-κB-Luc, pRL-TK, pTAL-Luc vectors (Promega Madison, WI) were transfected into the cells using Lipofectamine 3000 (Invitrogen, Carlsbad, CA) according to the manufacturer's instruction, followed by indicated treatment. Luciferase activity was assayed 48 hr after transfection using the Dual-Luciferase reporter assay system (Promega). Firefly luciferase activity was normalized to Renilla luciferase activity for each sample.

Immunoprecipitation

Cells were lysed in buffer containing 25 mM Tris●HCl pH 7.4, 150 mM NaCl, 1% NP-40, 1 mM EDTA, 5% glycerol and protease inhibitors. After incubated on ice for 5min with periodic mixing, the lysates were transferred into microcentrifuge tubes, centrifuged at 13,000 × g for 10min and the resulted supernatants were transferred to new tubes for protein concentration measurement and immunoprecipitation. The protein concentration of the lysates was measured by BCA method and equal amounts of protein were used for immunoprecipitation. For immunoprecipitation, antibody against p65 (1:100) or p300 (1:100) was added to the lysates for incubation overnight at 4°C, with rabbit IgG (1:100) as control antibody. Then Dynabeads® Protein A was added for incubation for another 1 hr at 4°C. After washing 5 times with the lysis buffer, the immunocomplexes were resuspended in protein loading buffer and were analyzed by immunoblotting.

Chromatin Immunoprecipitation Assay (ChIP)

ChIP assay was performed using EZ-Magna ChIP Chromatin Immunoprecipitation kit according to manufacturer's instructions. Briefly, 5 × 10^6 indicated CAFs were fixed in 1% formaldehyde for 10min at room temperature. Fixed cells were harvested, lysed and sonicated for 10 cycles of 10 s on/20 s off and 50% AMPL with Sonics VCX130 (Sonics & Materials, Inc, Newtown). Antibody against p65 (5ul per 1mg total protein) and rabbit IgG (2ul per 1mg total protein) were used for immunoprecipitation. The precipitated DNA was subjected to PCR amplification. The primer sequences used in ChIP assay were listed in Table S3.

Osteogenesis

For osteogenic differentiation, MSCs and fibroblasts were seeded at a density of 5 × $10^3/cm^2$. When the cells grew to 60% ~70% of confluence, osteogenic induction medium (L-DMEM containing 10%FBS, 0.1 μM dexamethasone, 50 μM vitamin C, and 10mM glycerophosphate) was added and replaced every 3 days. After 2 weeks of culture, the appearance of mineral nodules were analyzed by alizarin red S staining (2% of alizarin red S dissolved in distilled water with the pH value adjusted to 4.2).

Adipogenesis

MSCs and fibroblasts were seeded at a density of 5 × $10^3/cm^2$. When the cells grew to 100% of confluence, adipogenic induction medium (DMEM containing 10% FBS, 1 μM dexamethasone, 200 μM indomethacin, 0.5mM isobutylmethylxanthine and 10 μg/ml insulin was added and replaced every 3 days. After 2 weeks of culture, lipid accumulation was determined by Oil-red-O staining (0.5 g of Oil-red-O powder was dissolved in 100 mL of isopropanol).

PET/CT Imaging

The therapeutic effect on PDXs was assessed by ^{18}Fflourodeoxyglucose (^{18}F-FDG) Positron Emission Tomography/Computed Tomography(PET/CT) after eight weeks of docetaxel and GPR77 antibody combined treatment. Before PET/CT scanning, mice were fasted for 8 hr, anesthetized with 400mg/kg chloral hydrate, and injected with 5uci/g ^{18}F-FDG in 100 μL saline via tail vein. A 15minute static scan was performed 40min after ^{18}F-FDG injection with Inveon microPET/CT Scanner (Siemens, Germany). The micro PET images were corrected for attenuation, scatter, normalization, and camera dead time and co-registered with micro CT images. The tumor uptake of ^{18}F-FDG was calculated in terms of the standardized uptake value (SUV) in three-dimensional regions of interest (ROIs).

QUANTIFICATION AND STATISTICAL ANALYSIS

The information about statistical details and methods is indicated in the figure legends, text or methods. The measurements of all statistical values were performed using Graphpad Prism 5.0, unless otherwise described in the figure legends or methods. Error bars in the experiments indicate standard error of the mean (SEM) or standard deviation (SD) for a minimum of three independent experiments.

DATA AND SOFTWARE AVAILABILITY

The microarray data have been deposited in NCBI's Gene Expression Omnibus and are accessible through GEO Series accession number GEO: GSE108565 (https://www.ncbi.nlm.nih.gov/geo/query/acc.cgi?acc=GSE108565).

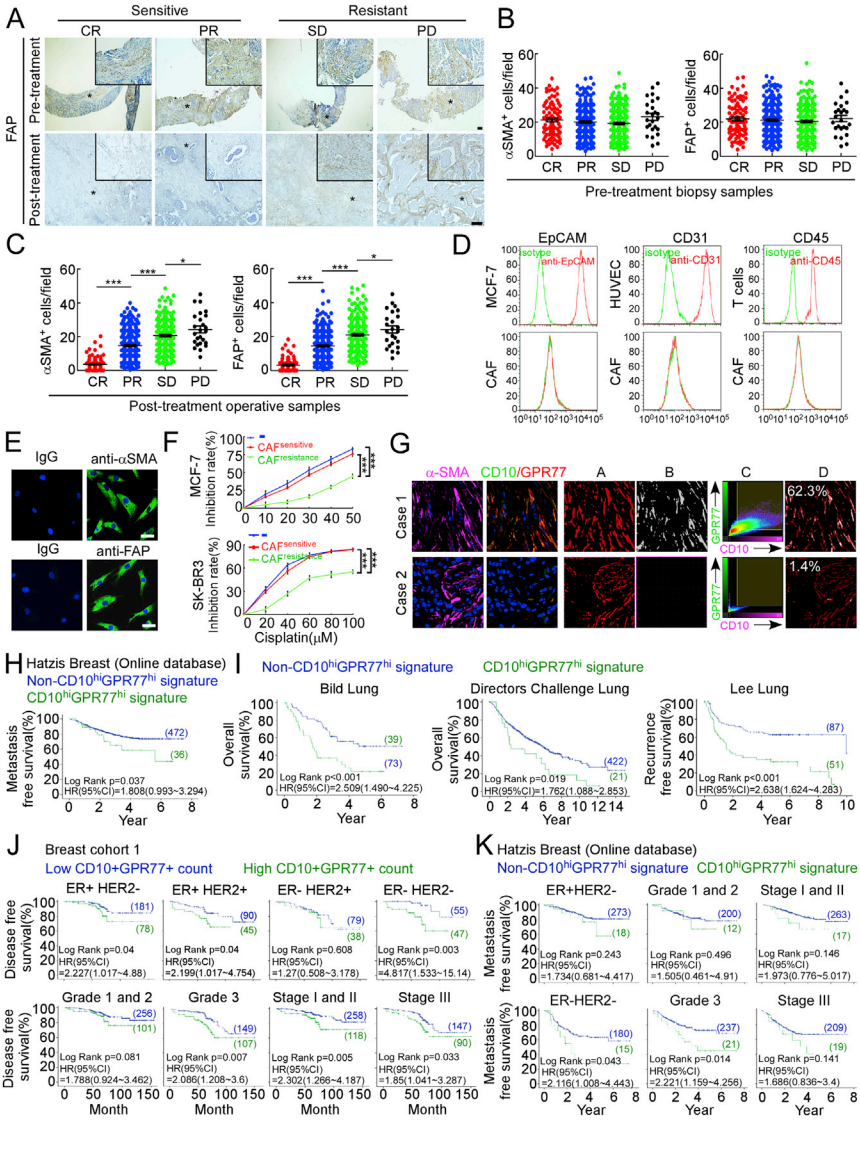

Figure S1. A CAF Subset with High CD10 and GPR77 Expression Correlates with Chemoresistance and Poor Survival in Breast and Lung Cancer Patients, Related to Figure 1

(A) Representative images of immunohistochemistry for FAP in breast cancer biopsies prior to neo-adjuvant chemotherapy and surgical resected breast cancer samples after neo-adjuvant chemotherapy. Asterisks indicated the area of higher magnification images. Scale bars, 50 μm.

(B and C) Quantification of α-SMA and FAP immunostaining in breast cancer biopsies prior to neo-adjuvant chemotherapy (B) and surgical resected breast cancer samples after neo-adjuvant chemotherapy (C) obtained from the same patients before and after neo-adjuvant chemotherapy. (CR, Complete Remission, n = 86; PR, Partial Remission, n = 258; SD, Stable Disease, n = 209; PD, Progressive Disease, n = 25). mean ± s.e.m., *$p < 0.05$; ***$p < 0.001$ by Student's t test.

(D) CAFs isolated from clinical samples were negative for EpCAM (epithelial marker), CD31 (endothelial marker) and CD45 (leukocyte marker), determined by flow cytometry. MCF-7 breast cancer cells, human umbilical vein endothelial cells (HUVEC) and human T lymphocytes were used as positive controls. Images for a representative sample were shown.

(E) Representative images showed that CAFs isolated from clinical samples expressed high level of myofibroblast markers, α-SMA and FAP. Scale bars, 50 μm.

(F) The growth inhibition rate of cisplatin on MCF-7 and SK-BR3 cells cultured alone or co-culture with indicated CAFs. CAFs were isolated from seven chemoresistant patients and seven chemosensitive ones before neo-adjuvant chemotherapy respectively. Mean ± s.e.m., ***$p < 0.001$ by Student's t test.

(G) The analysis method of the quantification of the proportion of $CD10^+GPR77^+$ CAFs in clinical samples analyzed by immunofluorescent staining using Imaris 9.0 Microscopy Image Analysis Software. Column 1 indicated the α-SMA staining and Column 2 indicated the CD10 and GPR77 double staining in the same tissue section. Column A to D showed the result analyzed by Imaris 9.0 Software. Column A indicated the α-SMA positive signal, Column B and C presented the co-locating signal of CD10 and GPR77, Column D displayed the co-locating area of CD10 and GPR77 in α-SMA positive area. The percentage of $CD10^+GPR77^+$ CAFs represents co-locating areas of CD10 and GPR77 divided by α-SMA positive area.

(H) Kaplan-Meier survival curves for breast cancer patients with or without high expression of both CD10 and GPR77 ($CD10^{hi}GPR77^{hi}$ signature and non-$CD10^{hi}GPR77^{hi}$ signature) in Hatzis breast cancer online database (n = 508). The optimal survival cut point was determined by X-Tile statistical software.

(legend continued on next page)

(l) Kaplan-Meier survival curves for NSCLC patients with or without high expression of both CD10 and GPR77 ($CD10^{hi}GPR77^{hi}$ signature and non-$CD10^{hi}GPR77^{hi}$ signature) in Bild Lung Cancer (n = 112), Directors Challenge lung cancer (n = 443) and Lee Lung Cancer (n = 138) online database. The optimal survival cut point was determined by X-Tile statistical software.

(J) Kaplan-Meier survival curves for breast cancer patients with low and high $CD10^{+}GPR77^{+}$ CAF abundance in different subtyping ($ER^{+}HER2^{-}$, $ER^{+}HER2^{+}$, $ER^{-}HER2^{+}$ and $ER^{-}HER2^{-}$), staging (stagel/IIand stage III) and histological grading (gradel/IIand grade III) of breast cancers in Breast cohort 1 (n = 613).

(K) Kaplan-Meier survival curves for breast cancer patients with or without overexpression of both CD10 and GPR77 genes in different subtyping ($ER^{+}HER2^{-}$, and $ER^{-}HER2^{-}$), staging (stagel/IIand stage III) and histological grading of breast cancers from the Hatzis breast cancer online database (n = 508). Analysis of $HER2^{+}$ subgroup was not performed due to limit patient number (n = 6).

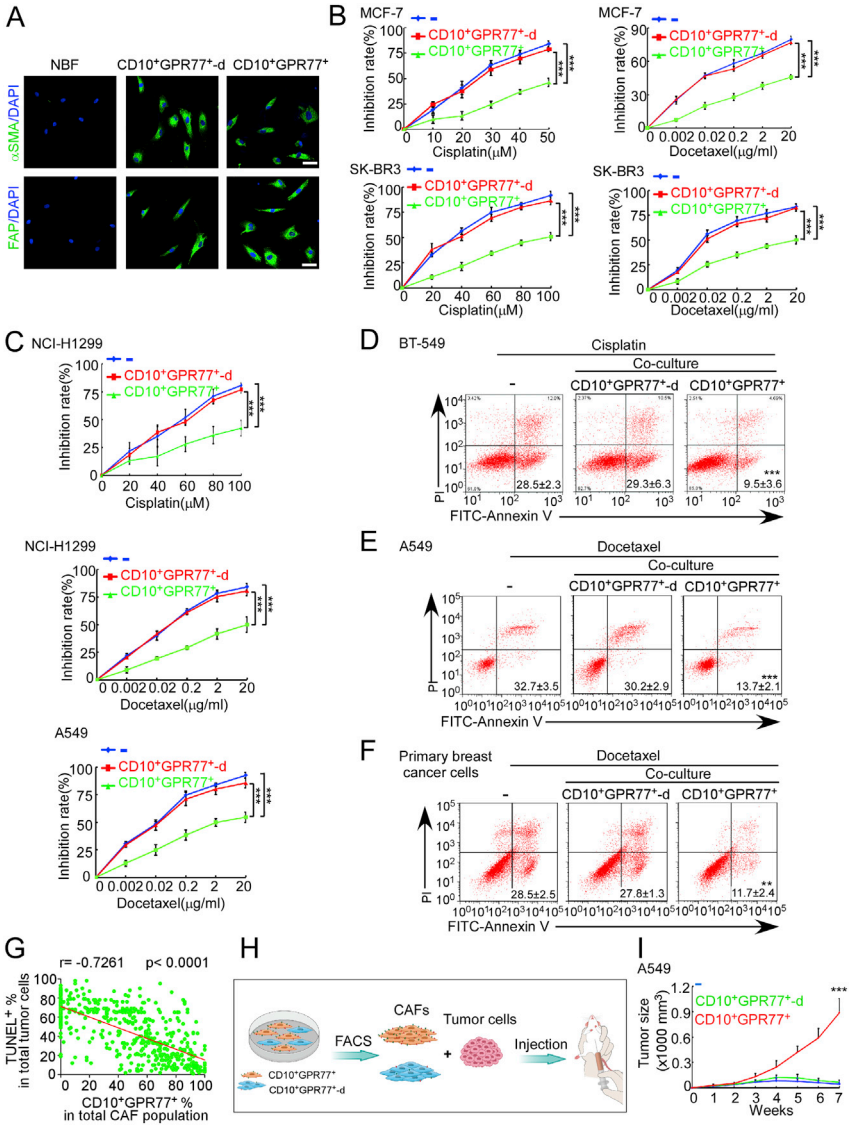

Figure S2. CD10$^+$GPR77$^+$ CAFs Induce Chemoresistance of Tumor Cells and Are Chemoresistant Themselves, Related to Figure 2

(A) CD10$^+$GPR77$^+$ CAFs and CD10$^+$GPR77$^+$-depleted (CD10$^+$GPR77$^+$-d) CAFs both expressed high level of α-SMA and FAP. Scale bars, 50 μm.

(B and C) The growth inhibition rates of cisplatin and docetaxel on indicated cancer cells cultured alone or co-culture with indicated CAFs. ***p < 0.001 by Student's t test.

(D) The proportion of apoptotic BT-549 breast cancer cells treated with cisplatin cultured alone or co-culture with CAFs. The proportions of Annexin V$^+$/PI$^-$ (early apoptosis) and Annexin V$^+$/PI$^+$ (late apoptosis) cells were shown. mean ± SEM, ***p < 0.001 by Student's t test compared with cancer cells cultured alone.

(E) The proportion of apoptotic A549 lung cancer cells treated with docetaxel cultured alone or co-culture with CAFs. Mean ± SEM, ***p < 0.001 by Student's t test compared with cancer cells cultured alone.

(F) Isolated primary breast cancer cells were cultured alone (-), or co-cultured with autologous CD10$^+$GPR77$^+$ CAFs, or paired CD10$^+$GPR77$^+$-depleted CAFs for 14 days. Afterward, docetaxel-induced apoptosis of cancer cells was assessed by flow cytometry. Mean ± SEM, **p < 0.01 by Student's t test compared with cancer cells cultured alone.

Three independent experiments were performed for CD10$^+$GPR77$^+$ CAFs and paired CD10$^+$GPR77$^+$-depleted CAFs isolated from each of the seven breast (B and D), four breast (F) and five NSCLC (C and E) patients. Mean ± SEM, ***p < 0.001 by Student's t test.

(G) The correlation between the percentage of CD10$^+$GPR77$^+$ CAFs and the percentage of TUNEL$^+$ tumor cells in breast cancer samples after neo-adjuvant chemotherapy (n = 578). Pearson's correlation coefficient r and p value were shown.

(H) Tumor cells were injected alone or co-injected with indicated CAFs at a ratio of 1:3 into the mammary fat pads of NOD.SCID mice. The approach schema was illustrated.

(I) A549 cells with or without indicated CAFs (1:3) were injected subcutaneously into NOD-SCID mice and treated with docetaxel weekly (n = 8 for each group). Tumor growth curves were monitored. ***p < 0.001 compared with (-) group by Student's t test at week 7.

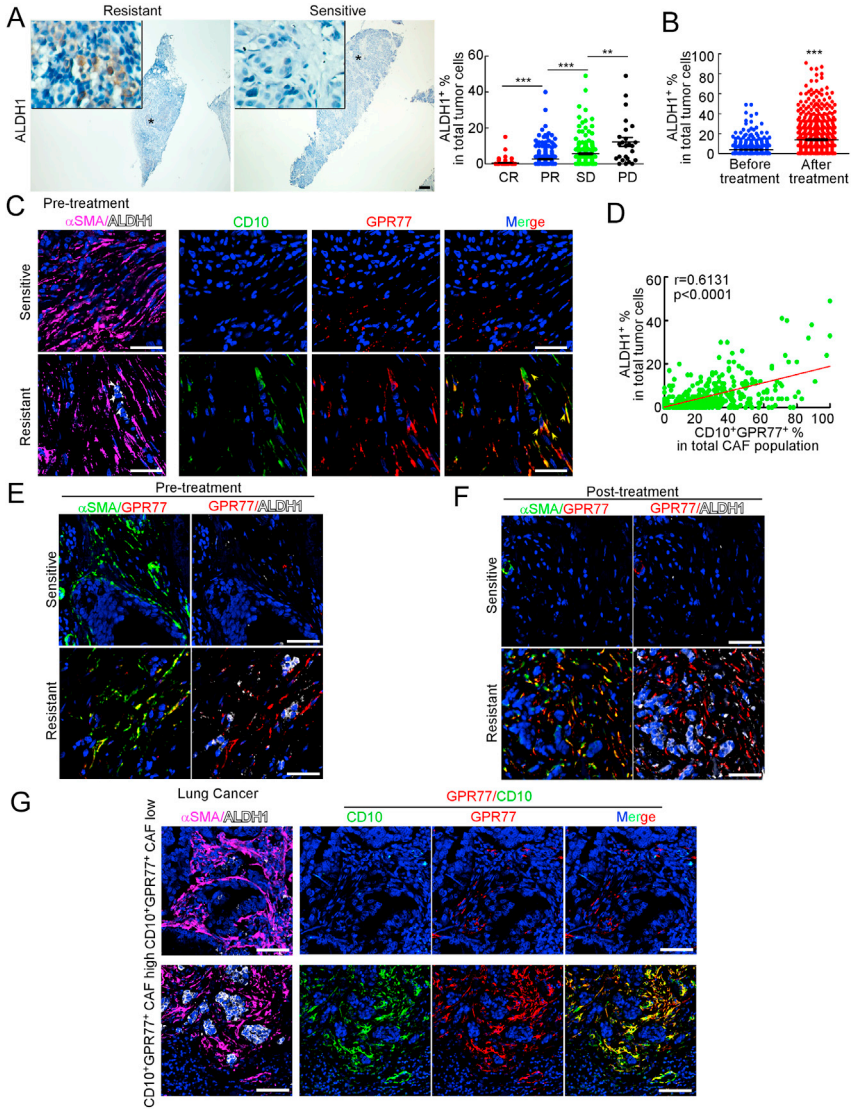

Figure S3. The Density of CD10$^+$GPR77$^+$ CAFs Correlates with CSC Abundance in Clinical Tumor Tissues, Related to Figure 3

(A) Representative images of ALDH1 immunohistochemistry and quantification of the ALDH1$^+$ tumor cell percentage in breast cancer biopsies before neo-adjuvant chemotherapy. Asterisks indicated the area of higher magnification images. Scale bars, 50 μm. (CR, Complete Remission, n = 86; PR, Partial Remission, n = 258; SD, Stable Disease, n = 209; PD, Progressive Disease, n = 25). Mean ± SEM, **p < 0.01; ***p < 0.001 by Student's t test.

(B) The percentage of ALDH1$^+$ tumor cells in post-treatment samples increased compared with those of pre-treatment biopsies. n = 578. ***p < 0.001 by Student's t test.

(C) Representative images of immunofluorescence of α-SMA, ALDH1, CD10 and GPR77 in serial sections of the pre-treatment breast cancer biopsies obtained before neoadjuvant chemotherapy. White arrows indicate ALDH1$^+$ cancer cells and yellow arrows indicate CD10$^+$ GPR77$^+$ CAFs. Scale bars, 50 μm.

(D) The correlation between the percentage of CD10$^+$GPR77$^+$ CAFs and the percentage of ALDH1$^+$ breast cancer cells in the biopsy samples before neoadjuvant chemotherapy. n = 578, Pearson's correlation coefficient r and p value were shown.

(E and F) Representative images of triple immunofluorescent staining of α-SMA, ALDH1 and GPR77 in breast cancer samples before and after neoadjuvant chemotherapy. Scale bars, 50 μm.

(G) Representative images of immunofluorescent staining of α-SMA, ALDH1, CD10 and GPR77 in serial sections of cancer samples of NSCLC. Scale bars, 50 μm.

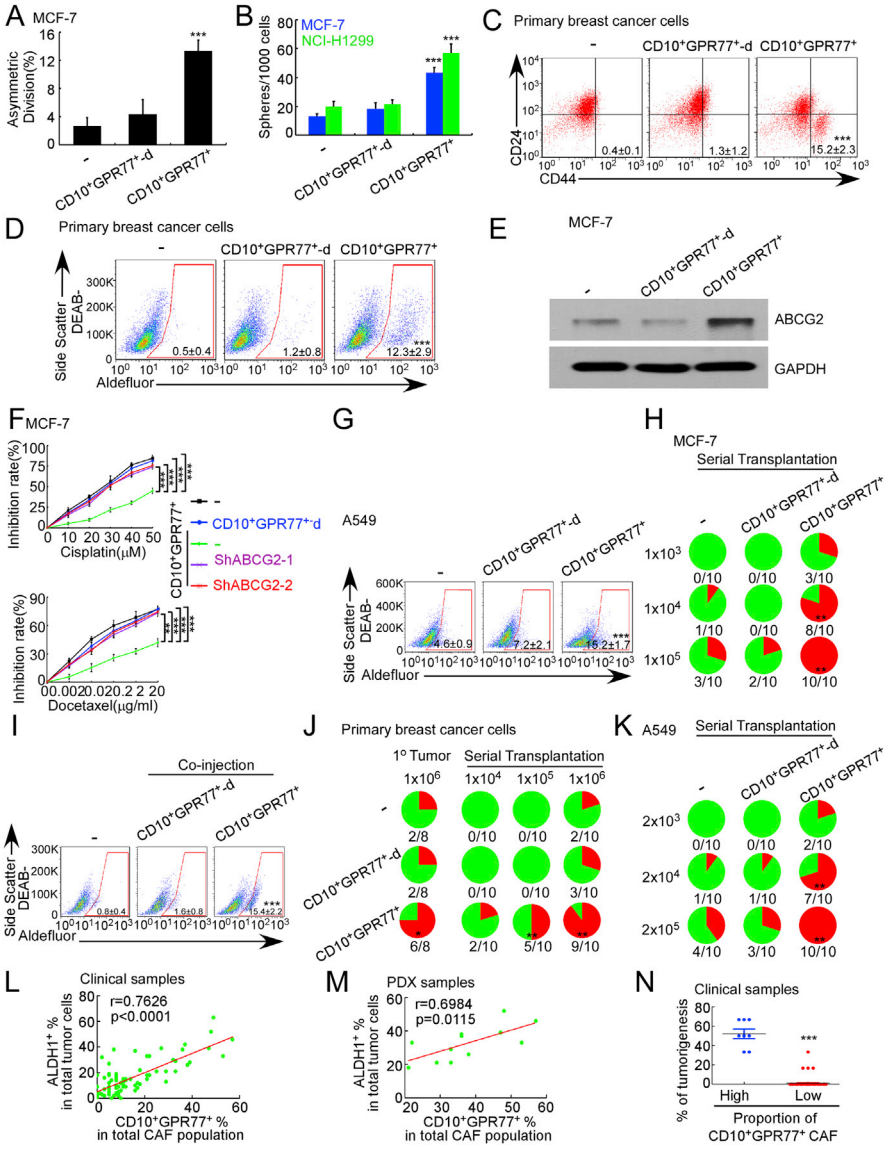

Figure S4. CD10$^+$GPR77$^+$ CAFs Enrich CSCs In Vitro and In Vivo, Related to Figure 3

(A) Quantification of asymmetric division in Figure 3D. Mean ± SEM ***p < 0.001 compared with tumor cells cultured alone by Student's t test.

(B) Quantification of sphere formation in Figure 3E. Mean ± SEM ***p < 0.001 compared with tumor cells cultured alone by Student's t test.

(C, D and G) Indicated cancer cell lines or autologous primary breast cancer cells were cultured alone (-), or co-cultured with CD10$^+$GPR77$^+$ CAFs or paired CD10$^+$GPR77$^+$-depleted (CD10$^+$GPR77$^+$-d) CAFs sorted from clinical samples of 5 breast (C), 4 breast (D) and 5 NSCLC (G) patients, respectively. The percentages of ALDH1$^+$ (D and G) and CD44$^+$CD24$^-$ (C) tumor cells were determined by flow cytometry. Three independent experiments were performed for each of the patients. Mean ± SEM ***p < 0.001 compared with tumor cells cultured alone by Student's t test.

(E) Representative western blotting images for the expression of ABCG2 in MCF-7 cells cultured alone (-), or co-cultured with CD10$^+$GPR77$^+$ CAFs or paired CD10$^+$GPR77$^+$-depleted CAFs. (n = 5)

(F) MCF-7 cells co-cultured with CD10$^+$GPR77$^+$ CAFs were transduced with ABCG2 shRNA and the growth inhibition rates of indicated cancer cells treated with cisplatin or docetaxel were assessed by MTT assay. n = 3, ***p < 0.001 by Student's t test.

(H) Incidences of tumorigenesis of the secondary tumor in serial transplantation models. MCF-7 cells were injected into the mammary fat pads of NOD.SCID mice alone or mixed with indicated CAFs (1:3). The xenografts were harvested 4 weeks later, and tumor cells were isolated and serially transplanted into NOD.SCID mice alone. **p < 0.01 compared with MCF-7 cells inoculated alone in the first inoculation by Fisher's exact test.

(I) The percentage of ALDH1$^+$ breast cancer cells in the first co-injected xenografts. n = 3, mean ± SEM ***p < 0.001 compared with MCF-7 cells inoculated alone.

(J) Incidence of tumorigenesis in primary breast cancer cells and autologous CAFs co-injection xenografts and the relevant serial transplantation models. *p < 0.05; **p < 0.01 compared with primary breast cancer cells inoculated alone in the first inoculation by Fisher's exact test.

(K) Incidences of tumorigenesis of the secondary tumor in serial transplantation models. A549 cells were injected subcutaneously into NOD.SCID mice alone or mixed with indicated CAFs (1:3) isolated from lung cancer patients. The xenografts were harvested 4 weeks later, and tumor cells were isolated and serially transplanted into NOD.SCID mice alone. **p < 0.01 compared with A549 cells inoculated alone in the first inoculation by Fisher's exact test.

(legend continued on next page)

(L and M) The correlation between the percentage of $CD10^{+}GPR77^{+}$ CAFs and $ALDH1^{+}$ tumor cells in breast cancer clinical samples (L, n = 82) and PDXs (M, n = 12). Pearson's correlation coefficient r and p values were shown. The representative pictures were shown in Figure 3I.

(N) The tumor formation rate of PDXs in high $CD10^{+}GPR77^{+}$ CAFs infiltrating breast cancer samples (> 30%) compared with those of low $CD10^{+}GPR77^{+}$ CAFs infiltrating ones. n = 8 for the high $CD10^{+}GPR77^{+}$ CAFs infiltrating group and n = 74 for the low $CD10^{+}GPR77^{+}$ CAFs infiltrating group. ***$p < 0.001$ by Mann Whitney test.

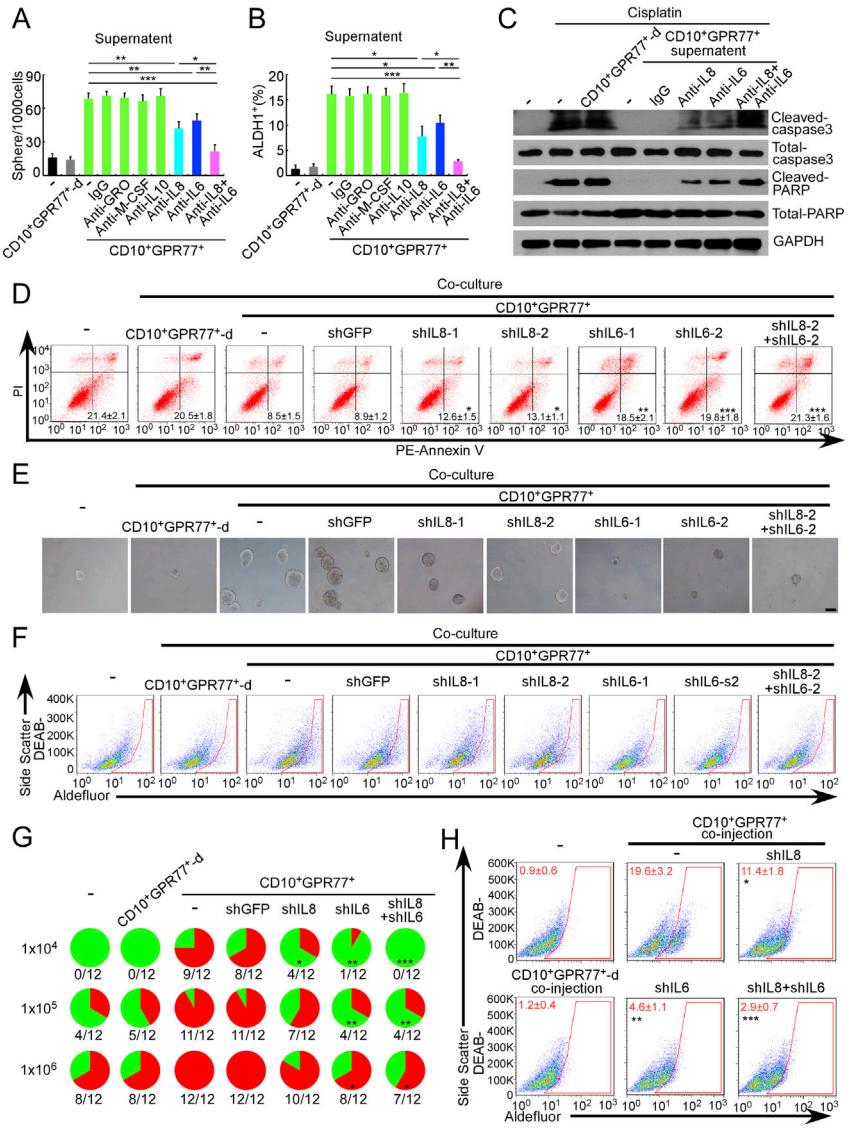

Figure S5. CD10$^+$GPR77$^+$ CAFs Induce CSCs Enrichment and Chemoresistance by Secreting IL-6 and IL-8, Related to Figure 4

(A and B) MCF-7 cells were treated with the supernatants of indicated CAFs with or without neutralizing antibodies against indicated cytokines. The proportions of mammosphere formation (A) and ALDH1$^+$ cells (B) were plotted. Three independent experiments were performed for each of the five patients, mean ± SEM, *p < 0.05; **p < 0.01 and ***p < 0.001 by Student's t test.

(C) SK-BR3 cells were treated with cisplatin in the presence or absence of the supernatants of indicated CAFs with or without neutralizing antibodies against IL-6 or/and IL-8. The representative images of western blotting showed the cleaved caspase-3 and PARP in SK-BR3 cells (n = 3).

(D-F) MCF-7 cells were cultured alone (-), co-cultured with CD10$^+$GPR77$^+$-depleted (CD10$^+$GPR77$^+$-d) CAFs, or with CD10$^+$GPR77$^+$ CAFs transduced without or with GFP shRNA, IL-6 or/and IL-8 shRNAs.

(D) The percentage of apoptotic MCF-7 cells after cisplatin treatment. Three independent experiments were performed for each of the five patients. Mean ± SEM, *p < 0.05; **p < 0.01; ***p < 0.001 as compared with MCF-7 cells co-cultured with untreated CD10$^+$GPR77$^+$ CAFs by Student's t test.

(E) Representative images of mammosphere formation. Scale bars, 100 μm. Quantitation is shown in Figure 4E.

(F) Representative plots of ALDH1$^+$ tumor cells determined by flow cytometry. Quantitation was shown in Figure 4E.

(G and H) MCF-7 cells were injected alone or co-injected with indicated CAFs at a ratio of 1:3 in NOD.SCID mice.

(G)The incidences of tumor formation after 2 months were shown. n = 12 per group. *p < 0.05; **p < 0.01 compared with the untreated CD10$^+$GPR77$^+$ CAF group by Fisher's exact test.

(H) Tumor cells were isolated from harvested xenografts inoculated by MCF-7 with or without indicated CAFs. The proportion of ALDH1$^+$ tumor cells was detected by flow cytometry. n = 4, mean ± SEM *p < 0.05; **p < 0.01; ***p < 0.001 compared with the untreated CD10$^+$GPR77$^+$ CAFs group by Student's t test.

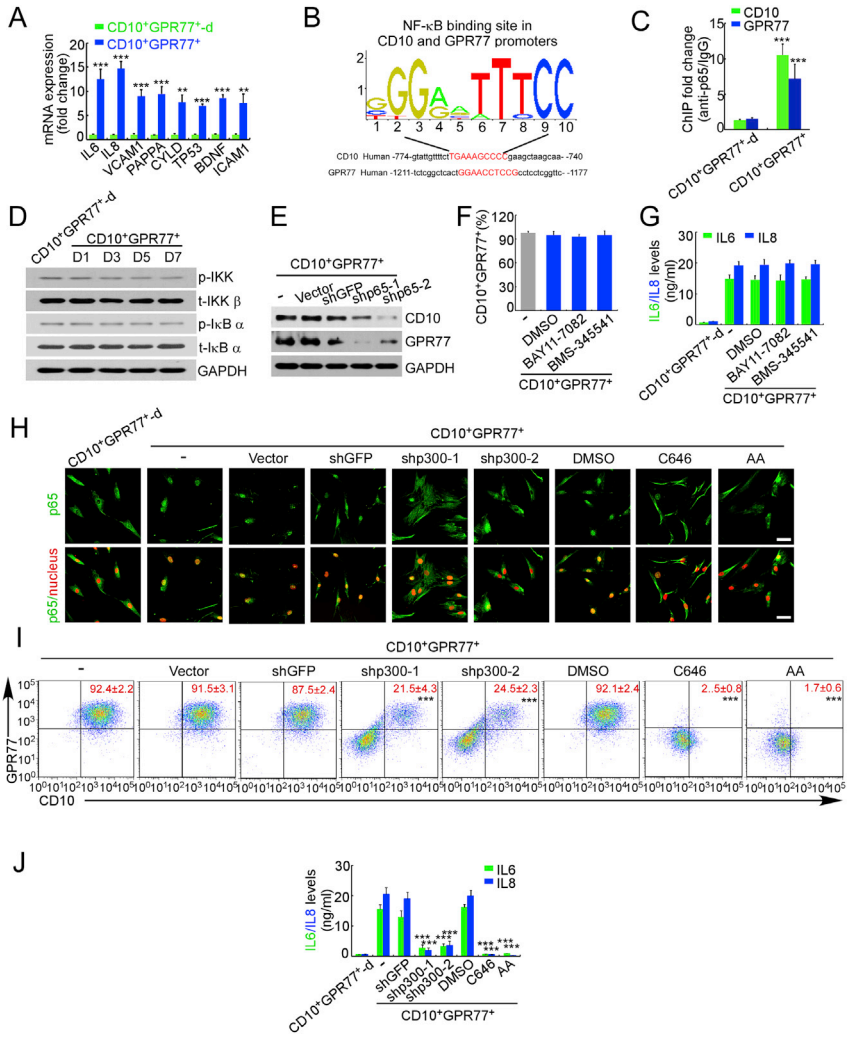

Figure S6. Prolonged NF-κB Activation via P300-mediated P65 Acetylation Maintains the Phenotypes and Functions of CD10$^+$GPR77$^+$ CAFs, Related to Figure 5

(A) Quantitative RT-PCR verified that a panel of NF-κB target genes were upregulated in CD10$^+$GPR77$^+$ CAFs compared with paired CD10$^+$GPR77$^+$-depleted CAFs (CD10$^+$GPR77$^+$-d). Mean ± SEM, ***p < 0.001 by Student's t test.

(B) P65-binding elements on the promoters of CD10 and GPR77 genes were predicted by JASPAR.

(C) Localizations of p65 to the promoters of CD10 and GPR77 genes in indicated CAFs were analyzed by ChIP assay using anti-p65 Ab or control IgG. Mean ± SEM, ***p < 0.001 by Student's t test.

(D) CD10$^+$GPR77$^+$ CAFs were cultured for indicated days. Paired CD10$^+$GPR77$^+$-depleted CAFs at day 1 served as control. Western blotting for total and phosphorylated IKK and IκBα was assessed.

(E) western blotting for CD10 and GPR77 in CD10$^+$GPR77$^+$ CAFs transduced without (-) or with p65 shRNA.

(F and G) CD10$^+$GPR77$^+$ CAFs were treated with IKK inhibitors (BAY 11-7082 or BMS-345541). Quantitation of CD10$^+$GPR77$^+$ CAF percentage determined by flow cytometry was shown in (F). IL-6 and IL-8 levels were detected by ELISA (G).

(H-J) CD10$^+$GPR77$^+$ CAFs were transduced without (-) or with p300 shRNA, or treated with p300 inhibitors (C646 or Anacardic Acid (AA), DMSO served as a negative control). Representative immunofluorescent images of p65 nuclear translocation of CAFs were shown in (H), and representative plots of CD10 and GPR77 expression determined by flow cytometry were shown in (I). IL-6 and IL-8 levels were detected by ELISA (J). Scale bars, 50 μm. Mean ± SEM, ***p < 0.001 compared with untreated CD10$^+$GPR77$^+$ CAFs by Student's t test.

A and F-J, 3 independent experiments were performed for each of the four patients. C-E, two replicates for each of the three patients.

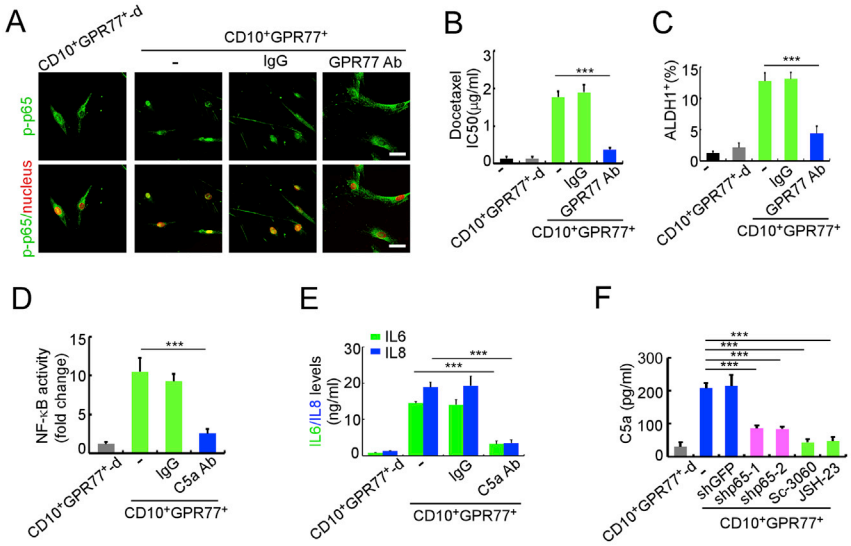

Figure S7. GPR77-Induced P65 Phosphorylation Is Prerequisite for Its Acetylation and Sustains NF-κB Activation in CD10$^+$GPR77$^+$ CAFs, Related to Figure 6

(A) CD10$^+$GPR77$^+$ CAFs were treated with control IgG or anti-GPR77 neutralizing antibody. P65 nuclear translocation was determined by immunofluorescent staining. Scale bars, 50 μm.

(B and C) MCF-7 cells were co-cultured with CD10$^+$GPR77$^+$ CAFs pretreated with control IgG or GPR77 neutralizing antibody. IC_{50} of docetaxel on MCF-7 cells was measured by MTT assay (B) and the percentage of ALDH1$^+$ cancer cells was determined by flow cytometry (C).

(D and E) NF-kB activity (D), IL6 and IL8 production (E) of CD10$^+$GPR77$^+$ CAFs treated with control IgG or C5a neutralizing antibody were determined by luciferase reporter assays and ELISA respectively.

(F) CD10$^+$GPR77$^+$ CAFs were transduced without (-) or with p65 shRNA or pretreated with inhibitors of NF-κB nuclear translocation (Sc-3060 and JSH-23). C5a in the supernatants of CD10$^+$GPR77$^+$-depleted CAFs (CD10$^+$GPR77$^+$-d) and CD10$^+$GPR77$^+$ CAFs was examined by ELISA.

Three independent experiments were performed for each of the four patients. Mean ± SEM, ***$p < 0.001$ compared with the untreated CD10$^+$GPR77$^+$ CAFs group by Student's t test.